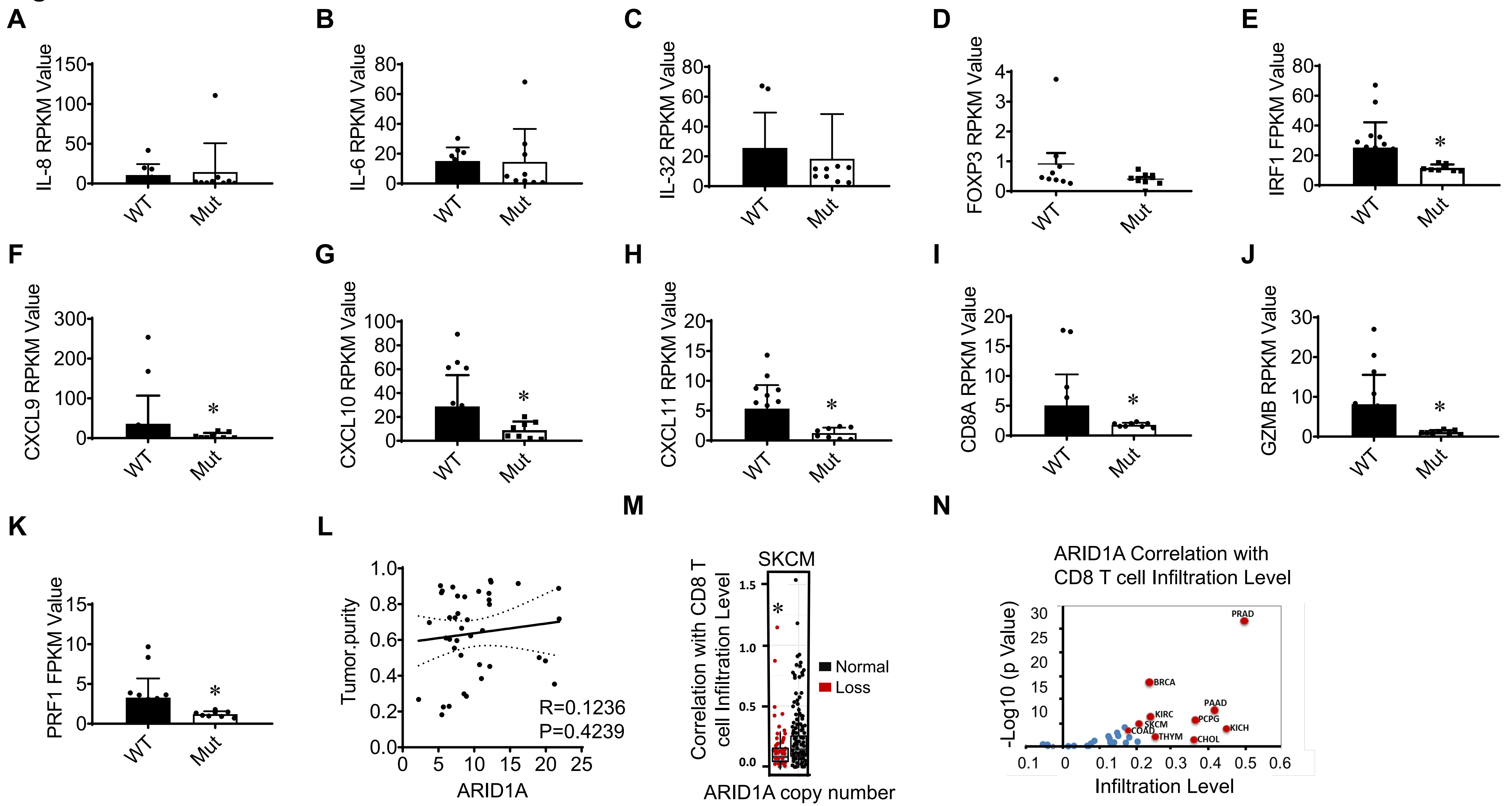


Fig. S1

Supplementary Figure 1 ARID1A gene status correlates with cancer immune signature

(A-D) Relationships between ARID1A mutations and immune associated gene expression. RNA-sequence was conducted in patients with ovarian clear cell carcinoma. 9 patients with ARID1A mutations, 9 patients with wild type ARID1A. Relationships between ARID1A mutations and CXCL8 (A), IL-6 (B), IL-32 (C), and FOXP3 (D) transcripts were analyzed. $P > 0.05$ (A-D).

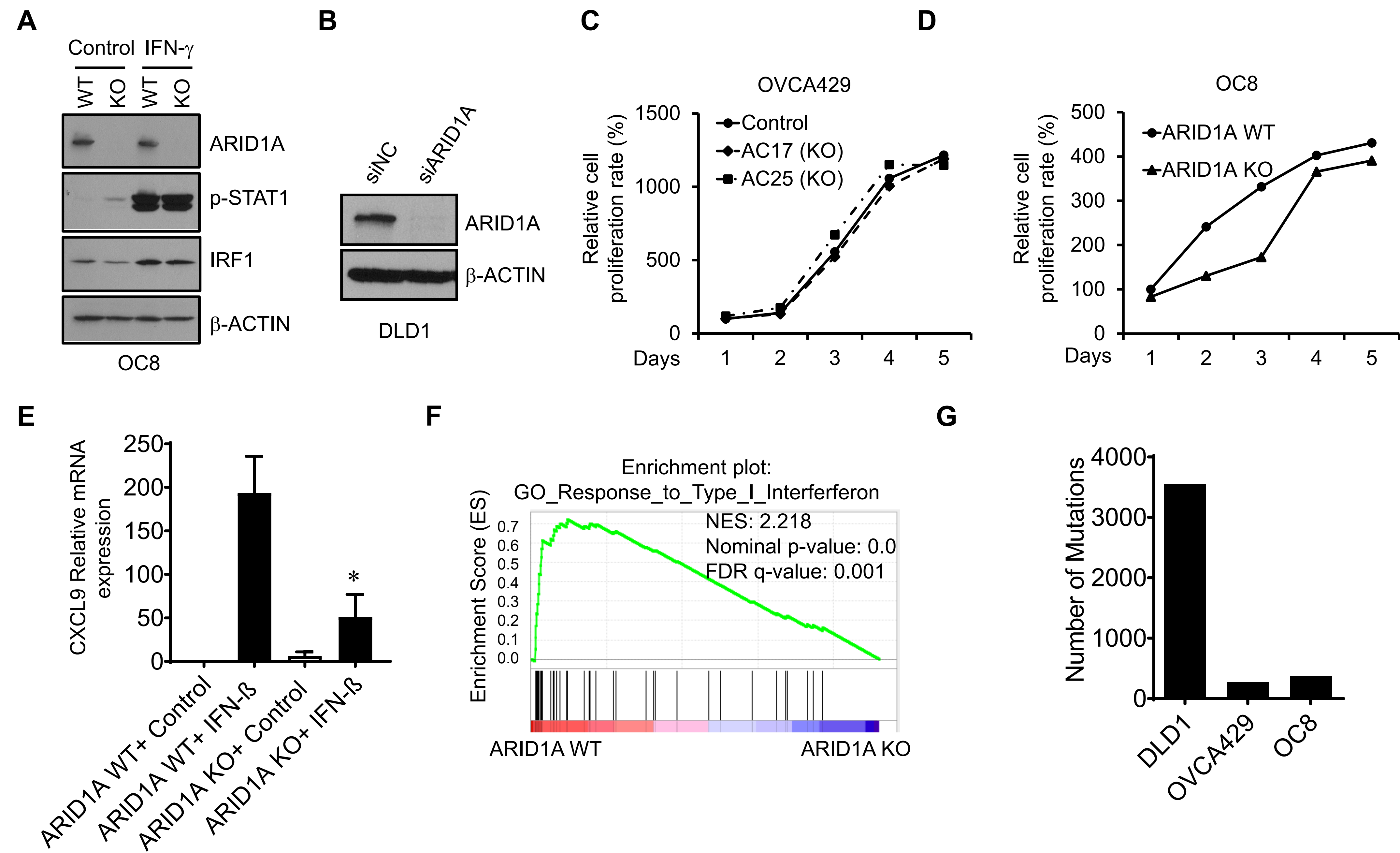
(E-K) Relationships between ARID1A mutations and immune associated gene expression in metastatic ovarian cancer patients of MET500 cohort. RNA-sequence was conducted in patients with metastatic ovarian cancer. 8 patients with ARID1A mutations; 16 patients with wild type ARID1A. Relationships between ARID1A mutations and IRF1 (E), CXCL9 (F), CXCL10 (G), CXCL11 (H), CD8A (I), GZMB (J), and PRF1 (K) transcripts were analyzed. *, $P < 0.05$ (E-K).

(L) Correlation between ARID1A gene expression levels and tumor purity in 47 wild type ARID1A metastatic melanoma patients. $P = 0.4$.

(M) Correlation between ARID1A somatic copy number loss and CD8+ T cells infiltration in melanoma (SKCM) of TCGA dataset. Correlation was analyzed with Tumor Immune Estimation Resource (TIMER) (<https://cistrome.shinyapps.io/timer/>). $P < 0.01$.

(N) Correlation between ARID1A expression and CD8+ T cells infiltration in TCGA datasets across cancer types. Correlation was analyzed with Tumor Immune Estimation Resource (TIMER) and adjusted with tumor purity. Each dot represents a cancer type in TCGA. The highlighted red dots were the most significant correlations (<https://cistrome.shinyapps.io/timer/>) (32, 94). PRAD: prostate adenocarcinoma, PAAD: Pancreatic Adenocarcinoma, KICH: kidney chromophobe, KIRC: kidney renal clear cell carcinoma, BRCA: breast carcinoma, PCPG: Pheochromocytoma and Paraganglioma, SKCM: skin cutaneous melanoma, COAD: colon adenocarcinoma, THYM: Thymoma, CHOL: Cholangiocarcinoma.

Fig. S2



H

Cell Line	Mutations	MMR	HR
DLD-1	MSH6, BRCA2, PIK3CA, APC, ARID1B, TP53, ASXL1, KRAS	Deficient	deficient
OVCA429	NF1, BRCA2 (germline pathogenic), MSH6 (heterozygous), TSC1	Proficient	deficient
OC8	BRAF, CDKN2A, TP53, CDK12, BRIP1 (heterozygous)	Proficient	proficient

Supplementary Figure 2 ARID1A mutations impair IFN signaling pathways in tumor

(A) Effects of ARID1A knockout on STAT1 activation and IRF1 induction in OC8 cells. One of 3 repeats is shown.

(B) ARID1A knockdown in DLD-1 cells. One of 3 repeats is shown.

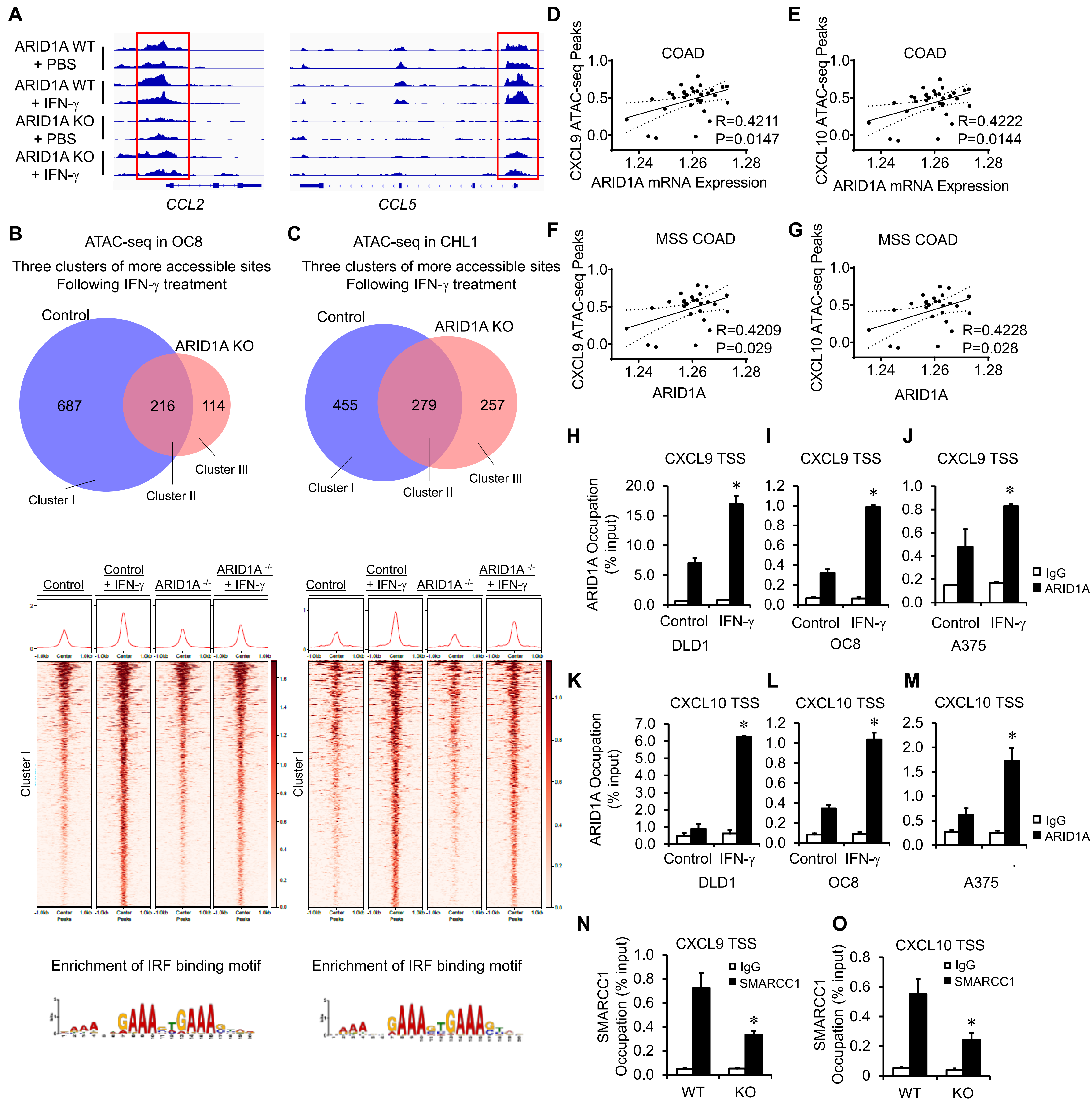
(C, D) Effects of ARID1A knockout on *in vitro* OVCA429 (C) and OC8 (D) growth.

(E) Effect of ARID1A on IFN- β -induced CXCL9 expression. ARID1A wild type and knock out ovarian clear cell cancer cells were treated with IFN- β for 6 hours. CXCL9 expression was quantified by real-time PCR. (Mean \pm SD, n = 3, *P < 0.05)

(F) GSEA plot of GO term type-I IFN response. Analysis was based on the RNA-seq data of ARID1A-deficient mouse colon epithelial cells (36), FDR q-value = 9.95e-4.

(G) Non-synonymous mutation numbers in DLD-1, OVCA428, and OC8 cell lines.

(H) Gene mutation examples in DLD-1, OVCA428, and OC8 cell lines. The data were from the whole exome sequencing.

Fig. S3

Supplementary Figure 3 ARID1A regulates IFN- γ -signaling gene chromatin accessibility

(A) Examples of IFN- γ -responsive sites with less accessibilities in ARID1A-deficient (KO) OVCA-429 cells. The graph shows accessible sites near CCL2 and CCL5.

(B) Top: Overlap between chromosomal regions that become more accessible following IFN- γ treatment in wild-type versus ARID1A knockout OC8 cells. Middle: Heatmaps illustrating open chromosomal regions in Cluster I. Aggregated peak intensities within 1kb center of chromatin regions with differential accessibility are shown. Bottom: IRF2-binding motif was among the most significantly enriched motifs.

(C) Top: Overlap between chromosomal regions that become more accessible following IFN- γ treatment in wild-type versus ARID1A knockout CHL1 cells. Middle: Heatmaps illustrating open chromosomal regions in Cluster I. Aggregated peak intensities within 1kb center of chromatin regions with differential accessibility are shown. Bottom: IRF2-binding motif was among the most significantly enriched motifs.

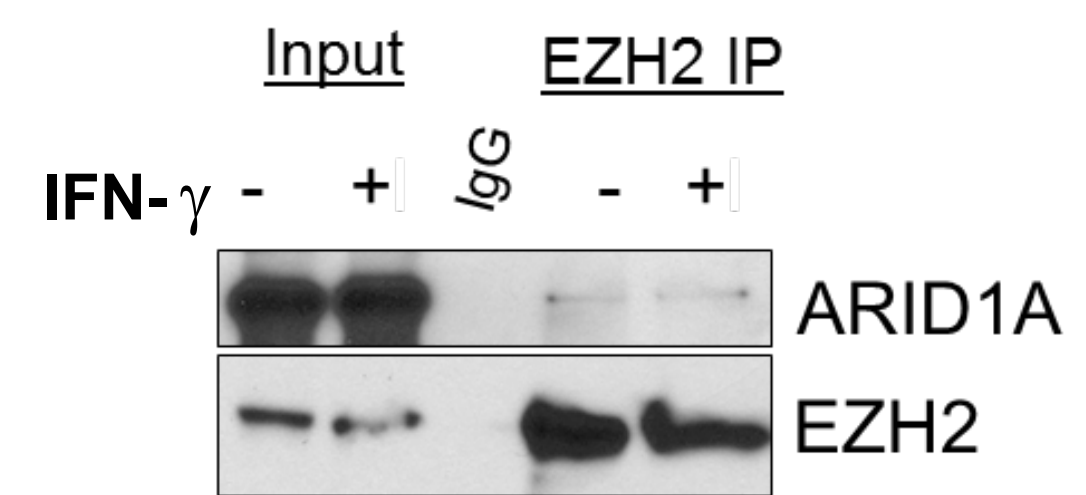
(D-G) Correlation between ARID1A mRNA expression and average chromatin accessibility peaks near CXCL9 gene (221 peaks) (D, F) and CXCL10 (219 peaks) (E, G) in patients with wild type ARID1A colon cancer. Analysis was conducted in 33 patients (D, E) and 27 microsatellite stable (MSS) patients (F, G). Patients with microsatellite instability (MSI) were included (n = 33) (D, E) or excluded (F, G) (n = 27) in the analysis. Each dot represents an individual donor. ARID1A gene expression is log transformed. P=0.0147 (D), P = 0.0144 (E), P = 0.029 (F), P = 0.028 (G).

(H-M) ARID1A occupation on CXCL9 (H, I, J) and CXCL10 (K, L, M) promoters in IFN- γ -stimulated DLD-1, OC8, and A375 cells. ChIP was performed with ARID1A antibody. (mean \pm SD, n = 3, *P < 0.05)

(N-O) Effect of ARID1A on the BAF component occupancies on the promoters of CXCL9 (N) and CXCL10 (O). ChIP was performed with SMARCC1 antibody in IFN- γ -stimulated ARID1A wild type or knockout (KO) OC8. Results are shown as the occupation of SMARCC1 at CXCL9 and CXCL10 promoters. Data were normalized to the input. (mean \pm SD, n = 3, *P < 0.05)

Fig. S4

A



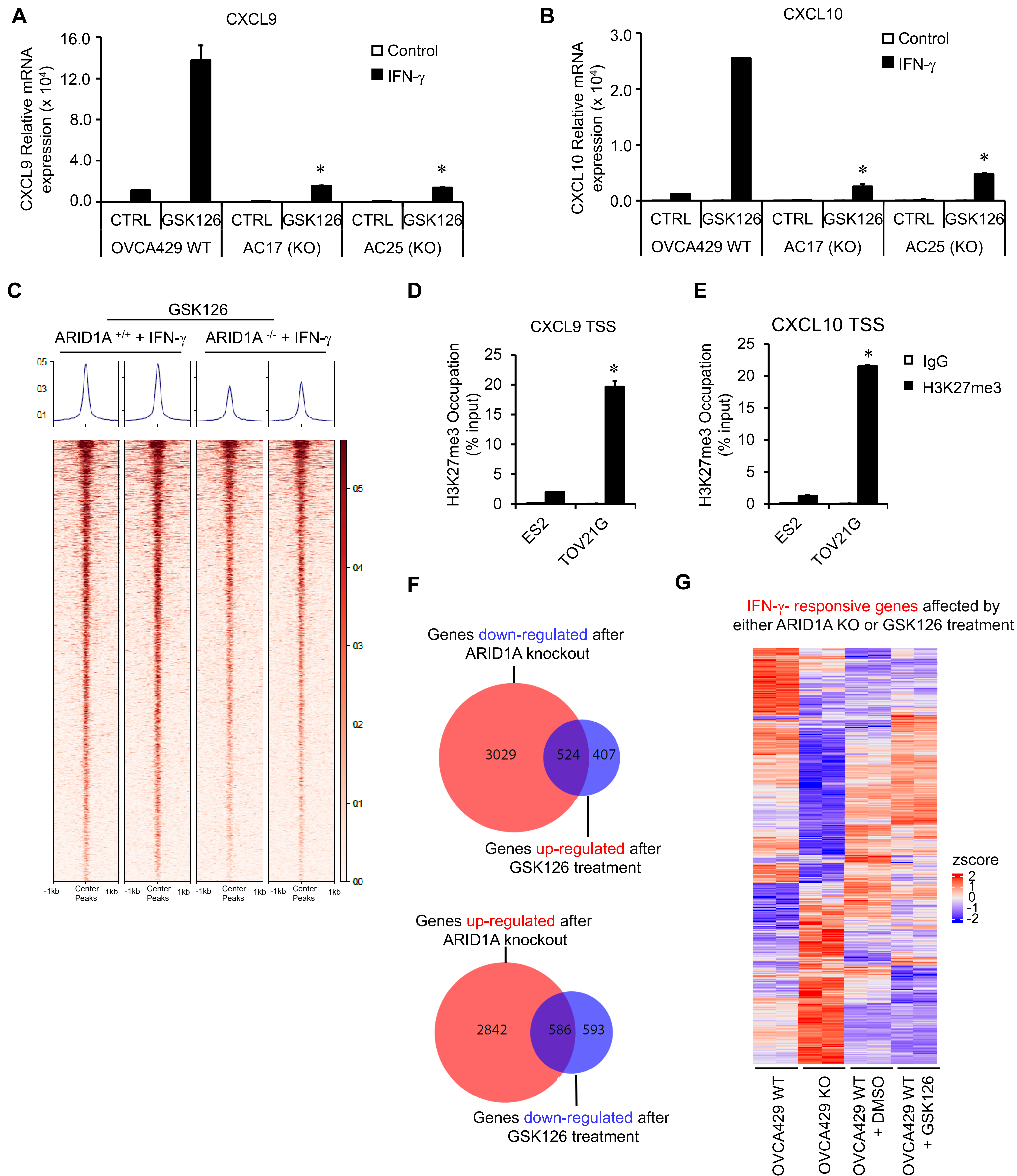
B



Supplementary Figure 4 ARID1A biochemically interacts with EZH2

(A) Interaction between ARID1A and EZH2 in HCT116 colon cancer cells. Endogenous EZH2 was immunoprecipitated with anti-EZH2 and ARID1A was probed with Western blot. One of 3 is shown.

(B) *In vivo* interaction between ARID1A and EZH2. OVCA429 ARID1A knockout cells expressing flag tagged wild type ARID1A were injected into NSG mice. The tumor was used to conduct immunoprecipitation with EZH2 antibody, and probed with Flag antibody.

Fig. S5

Supplementary Figure 5 ARID1A functionally interacts with EZH2

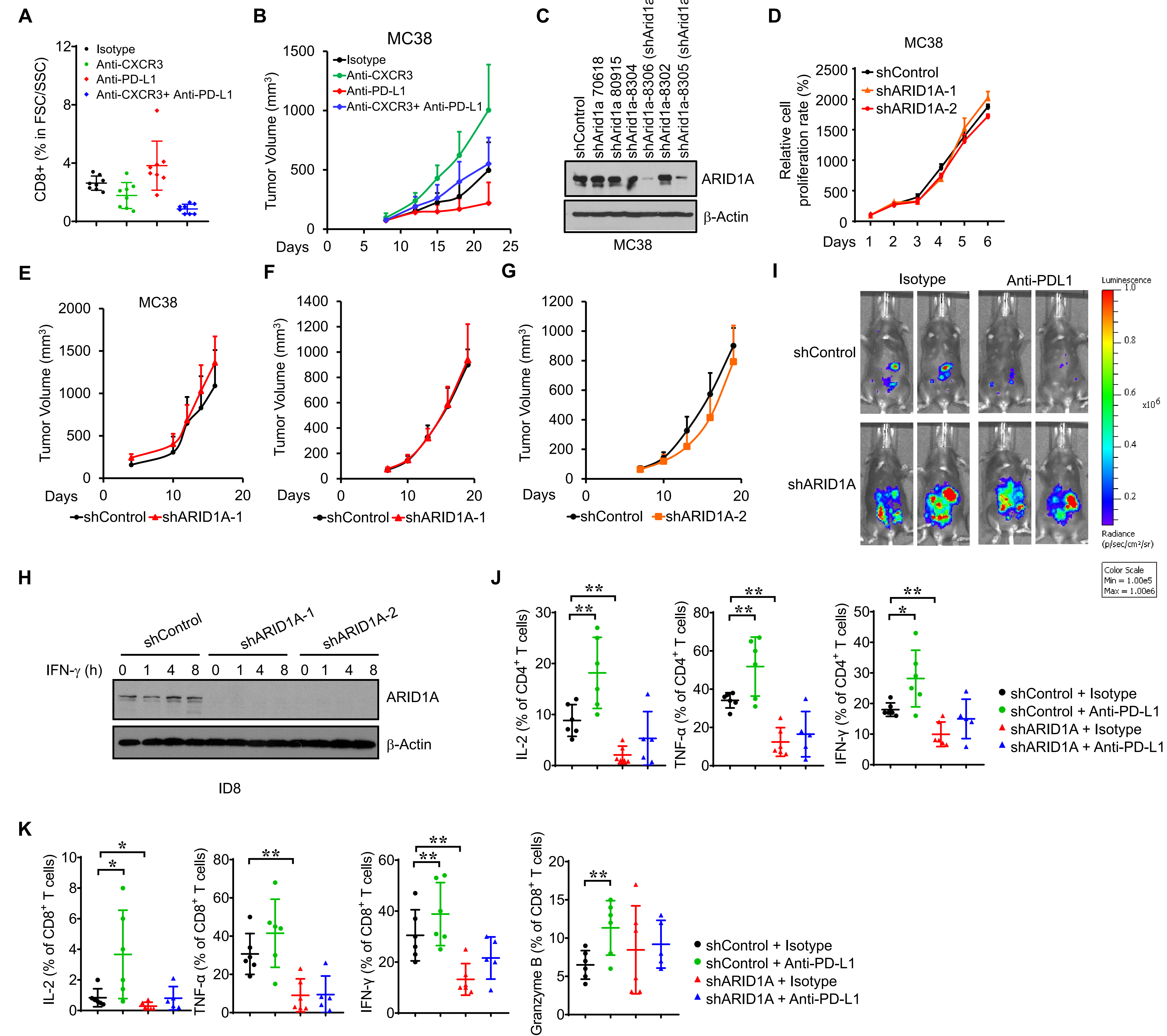
(A-B) Effect of ARID1A on EZH2-mediated Th1-type chemokine repression in ovarian cancer cells. Parental OVCA429 cells (WT), ARID1A knockout (AC17 and AC25 KO) cells were treated with GSK126 and stimulated with IFN- γ for 12 hours. CXCL9 (A) and CXCL10 (B) transcripts were quantified by real time PCR. (n = 3, *P < 0.05, Student's t tests).

(C) Chromatin accessibility heatmaps depicting IFN- γ -responsive chromosomal sites under GSK126-treated conditions, in ARID1A wild type or knock out OVCA429 cells.

(D-E) Effect of ARID1A on H3K27me3 mediated Th1-type chemokine repression in ovarian cancer cells. ES2 cells with ARID1A wild type or TOV21G cells with ARID1A mutant were treated with IFN- γ for 6 hours. H3K27me3 CHIP was performed. H3K27me3 levels on the promoters of CXCL9 and CXCL10 were normalized to the input. Mean \pm SD, n = 3, Student's t tests, *P = 0.036 (D); *P = 0.030 (E).

(F) Venn diagram indicating the overlap between ARID1A regulated genes (red) or GSK126 regulated genes (blue) in reverse direction following IFN- γ -stimulated OVCA429 cells.

(G) Gene expression heatmaps of IFN- γ -responsive genes which have significant changes with ARID1A deletion and GSK126 treatment.

Fig. S6

Supplementary 6 ARID1A regulates spontaneous tumor immunity *in vivo*

(A-B) Effect of CXCR3 blockade on anti-PD-L1 therapy in MC38 bearing mice. MC38 bearing mice were treated with isotype, anti-CXCR3, anti-PD-L1 or the combination. Tumor infiltrating CD8⁺ T cells were detected by flow cytometry analysis (A). Tumor volume was monitored (B). Mean \pm SD, n = 8-10. Mann-Whitney U test, *P < 0.05, **P < 0.01.

(C) Knockdown ARID1A in MC38 cells. ARID1A was knocked down with different shRNAs. shARID1A clones (shARID1A-1 and shARID1A-2) were selected based on Western blotting. One of 3 repeats is shown.

(D) Effect of shARID1A on MC38 cell proliferation *in vitro*. Results are expressed as relative cell proliferation rate compared to day 1. Mean \pm SD, n = 5.

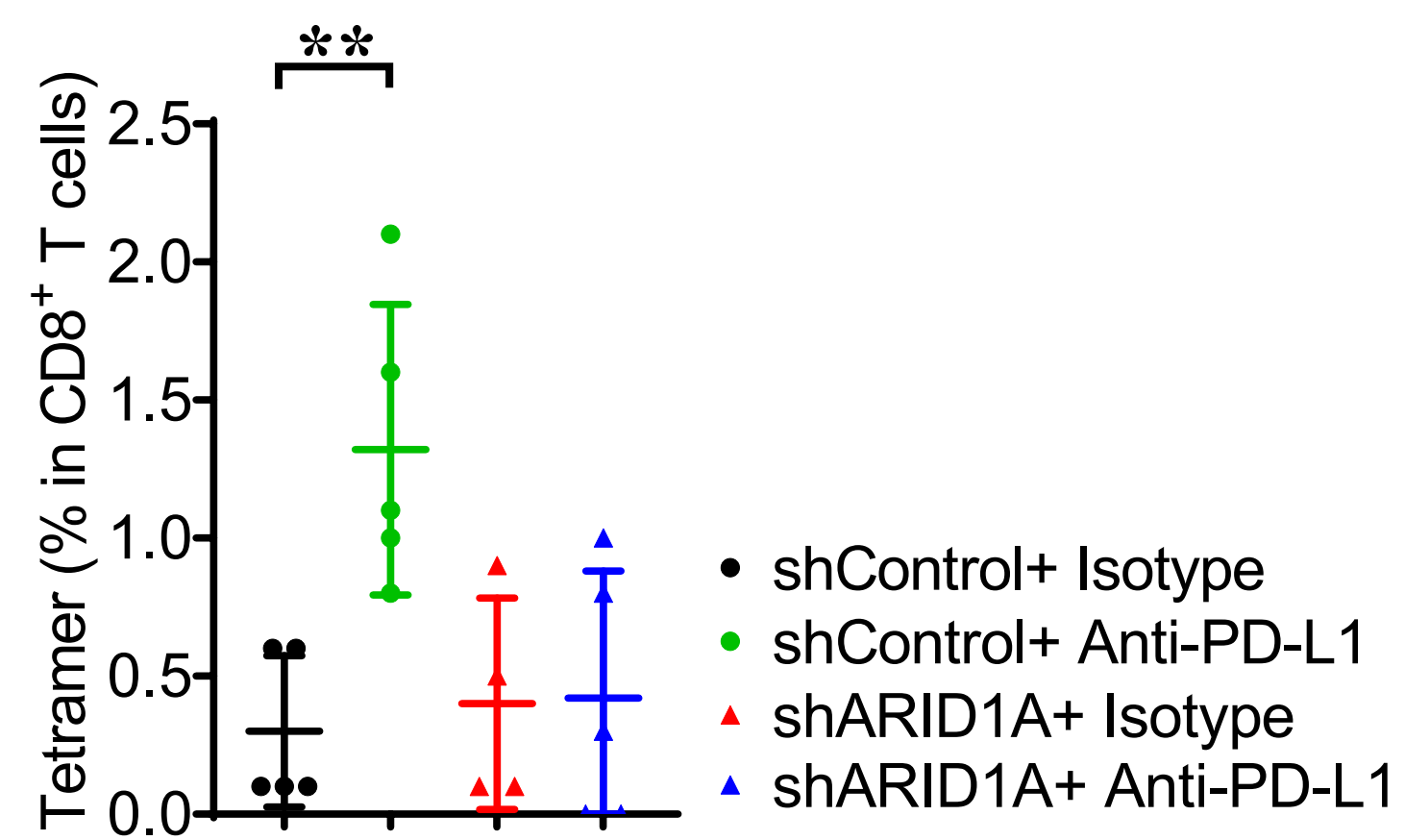
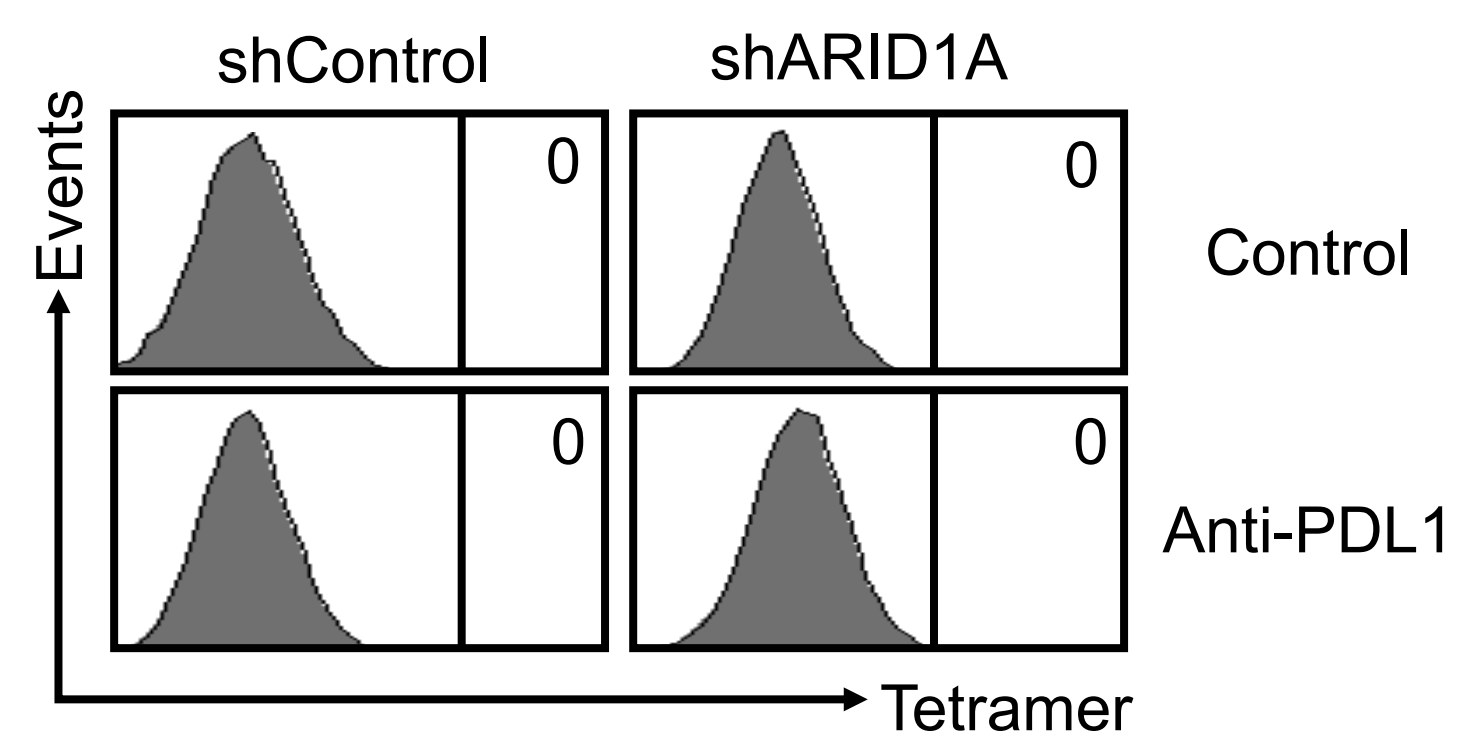
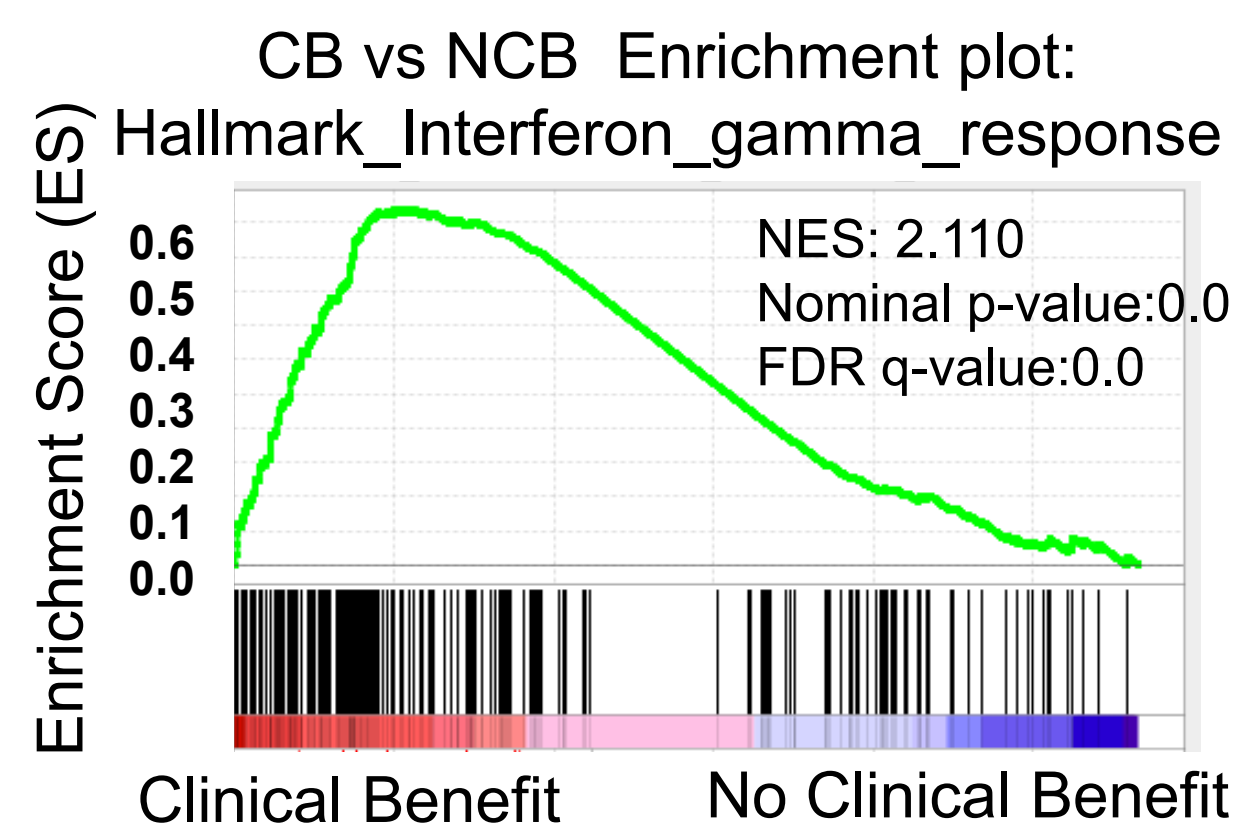
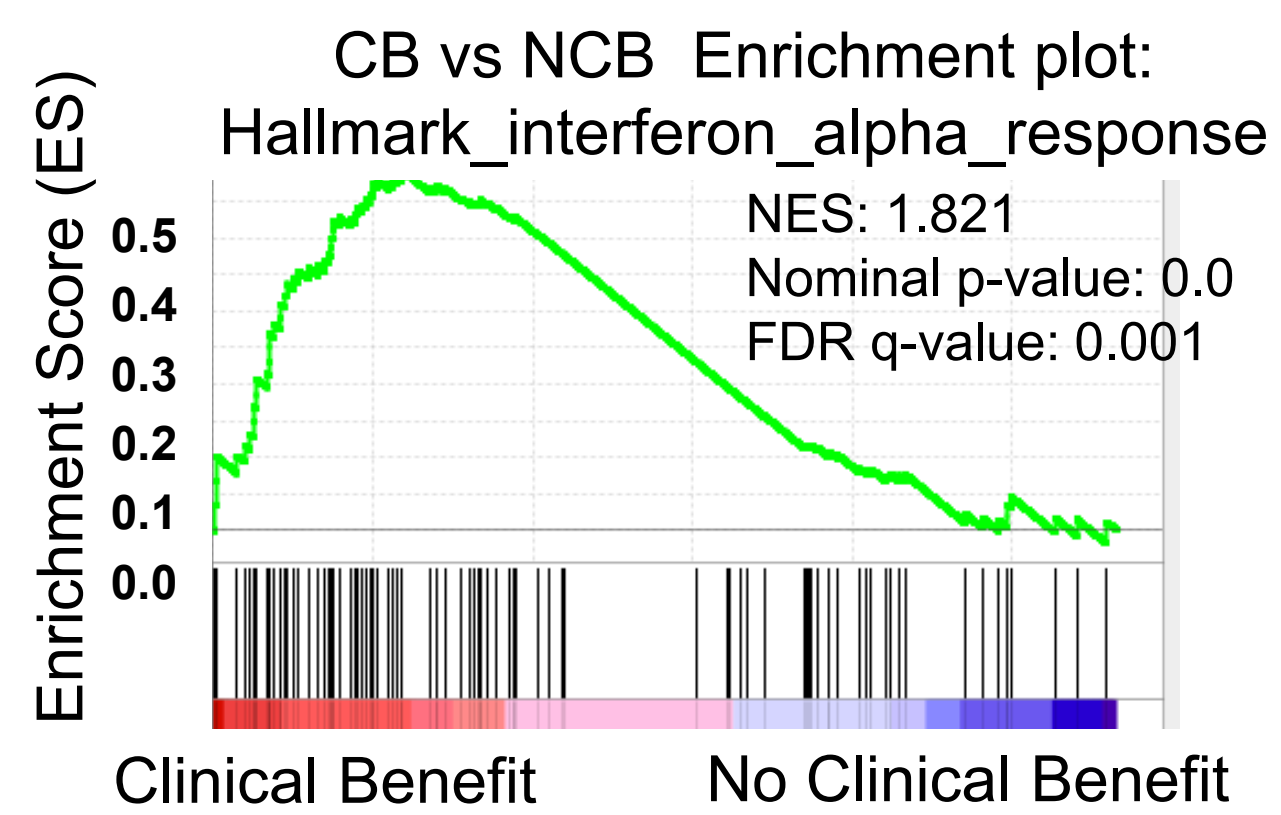
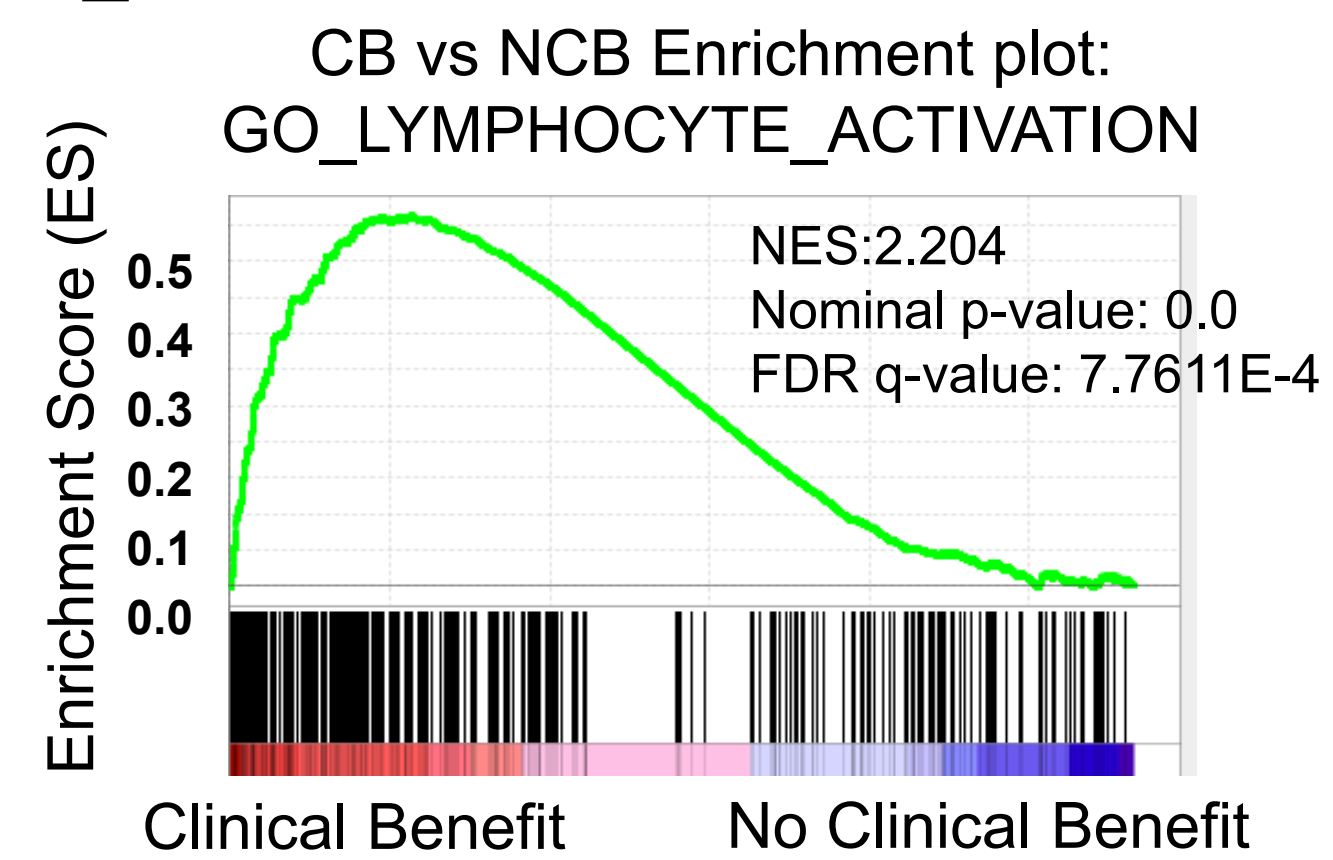
(E) Effect of shARID1A on MC38 growth *in vivo*. MC38 tumor cells were inoculated into NSG mice. Tumor volume was monitored. Mean \pm SD, n = 5.

(F-G) Effects of CD8 depletion on shARID1A MC38 colon cancer cell growth in C57BL/6 mice. C57BL/6 mice were inoculated with MC38 expressing shARID1A-1 (F), shARID1A-2 (G), or control vectors. Mice were treated with isotype or anti-mCD8. Tumor volume was monitored. Mean \pm SD, n = 7-8, Mann-Whitney U test (F). P > 0.05.

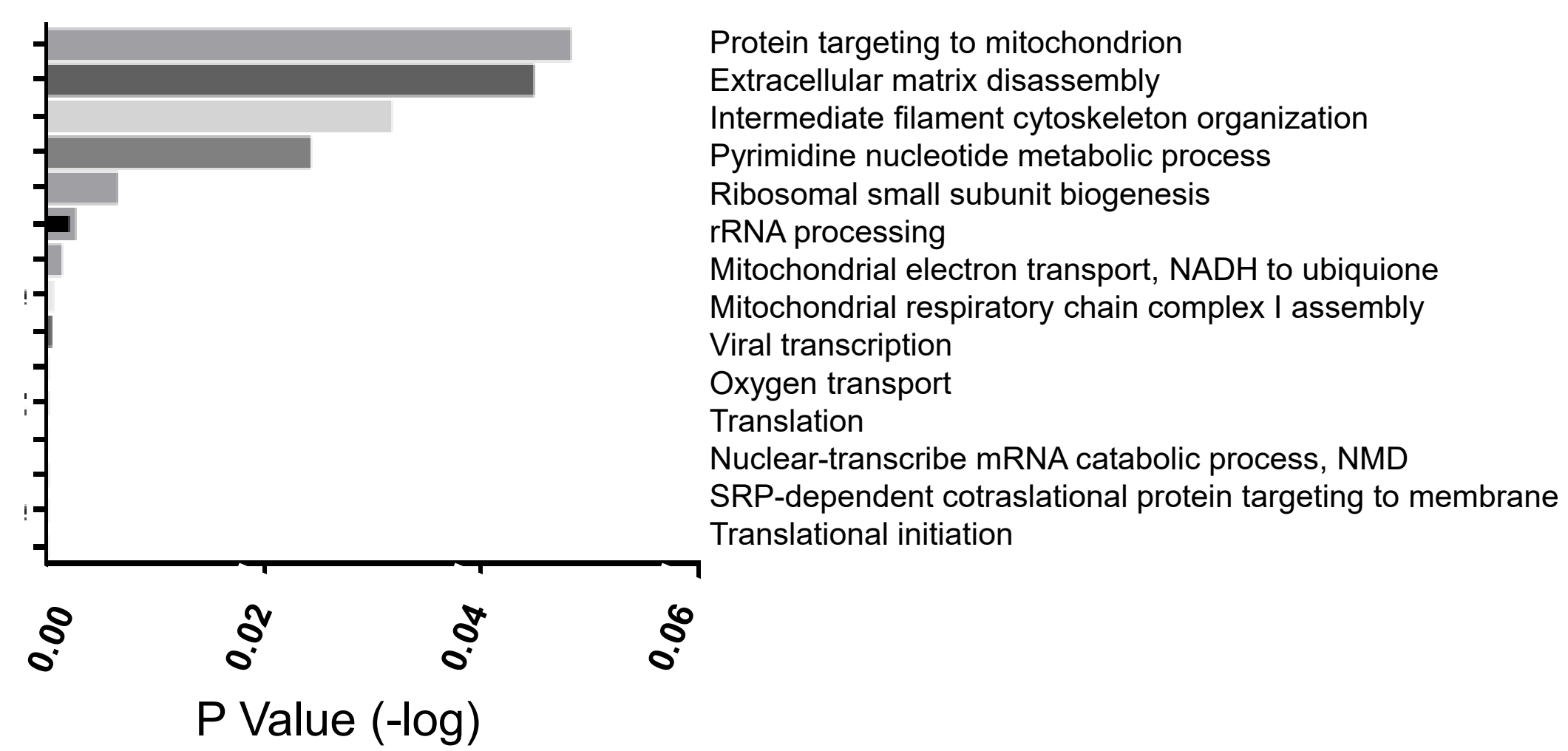
(H) Knockdown ARID1A in ID8 cells. ARID1A was knocked down in ID8 cells with different shRNAs. ID8 cells were stimulated with IFN- γ for 24 hours. Knockdown efficacy was tested by Western blotting. One of 3 repeats is shown.

(I) Representative photon flux from C57BL/6 mice bearing ID8 tumors.

(J-K) Quantification of effector cytokines in ID8 tumor infiltrating CD4⁺ (J) and CD8⁺ (K) T cells. Mean \pm SD, n = 5-6, Mann-Whitney U test, *P < 0.05; **P < 0.01.

Fig. S7**A****B****C****D****E****F**

Enriched Biological Functions in NCB Patients



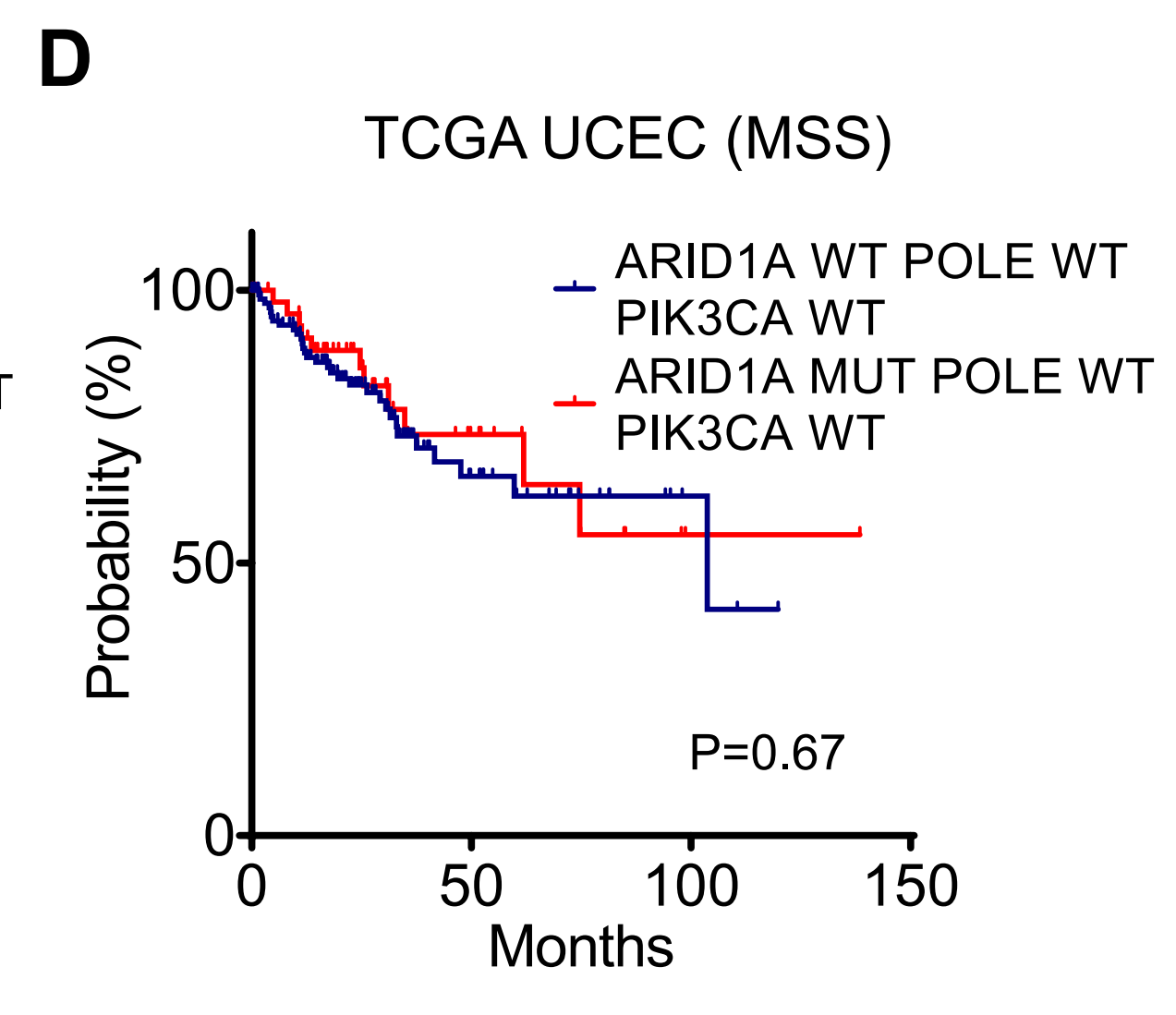
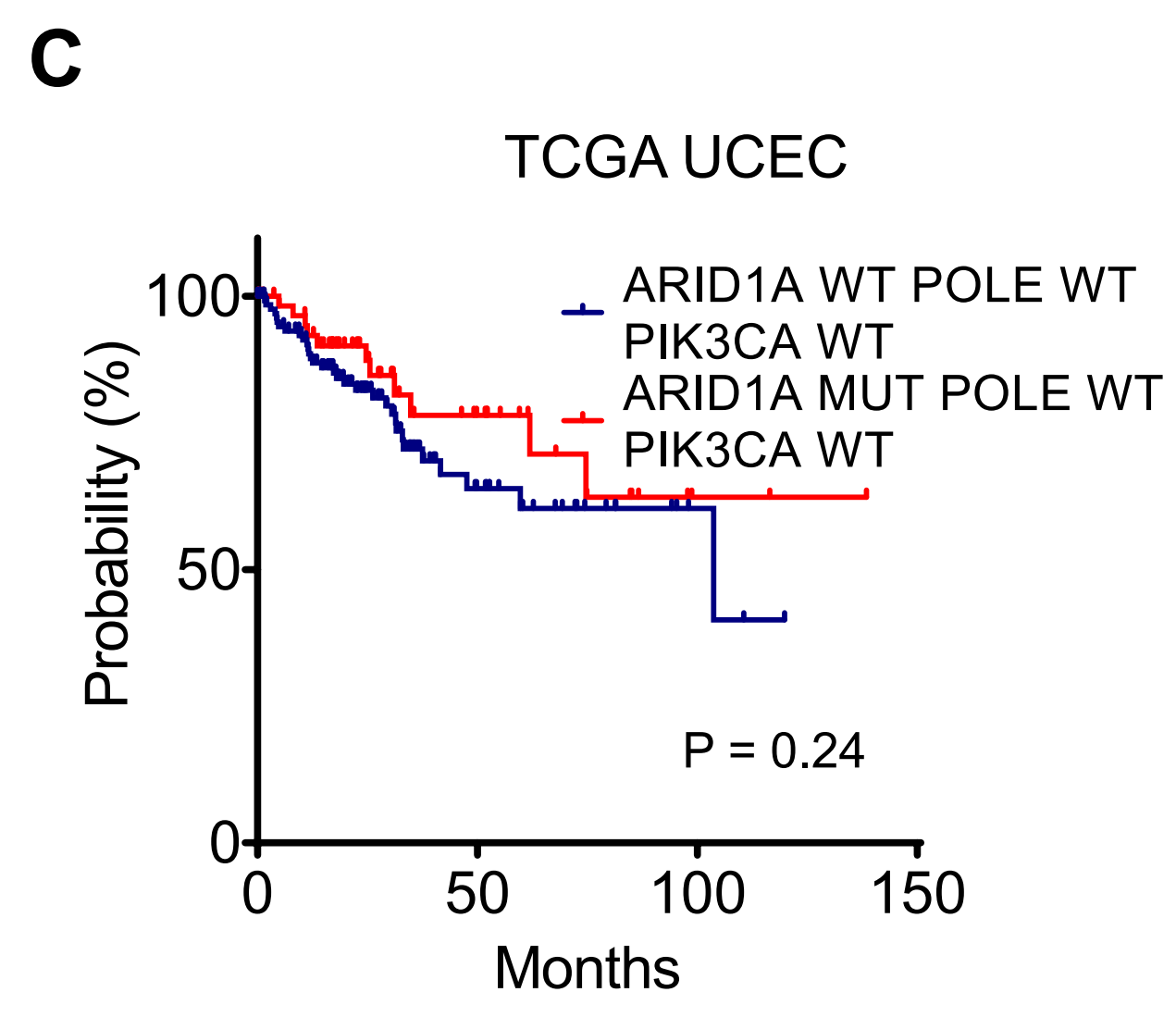
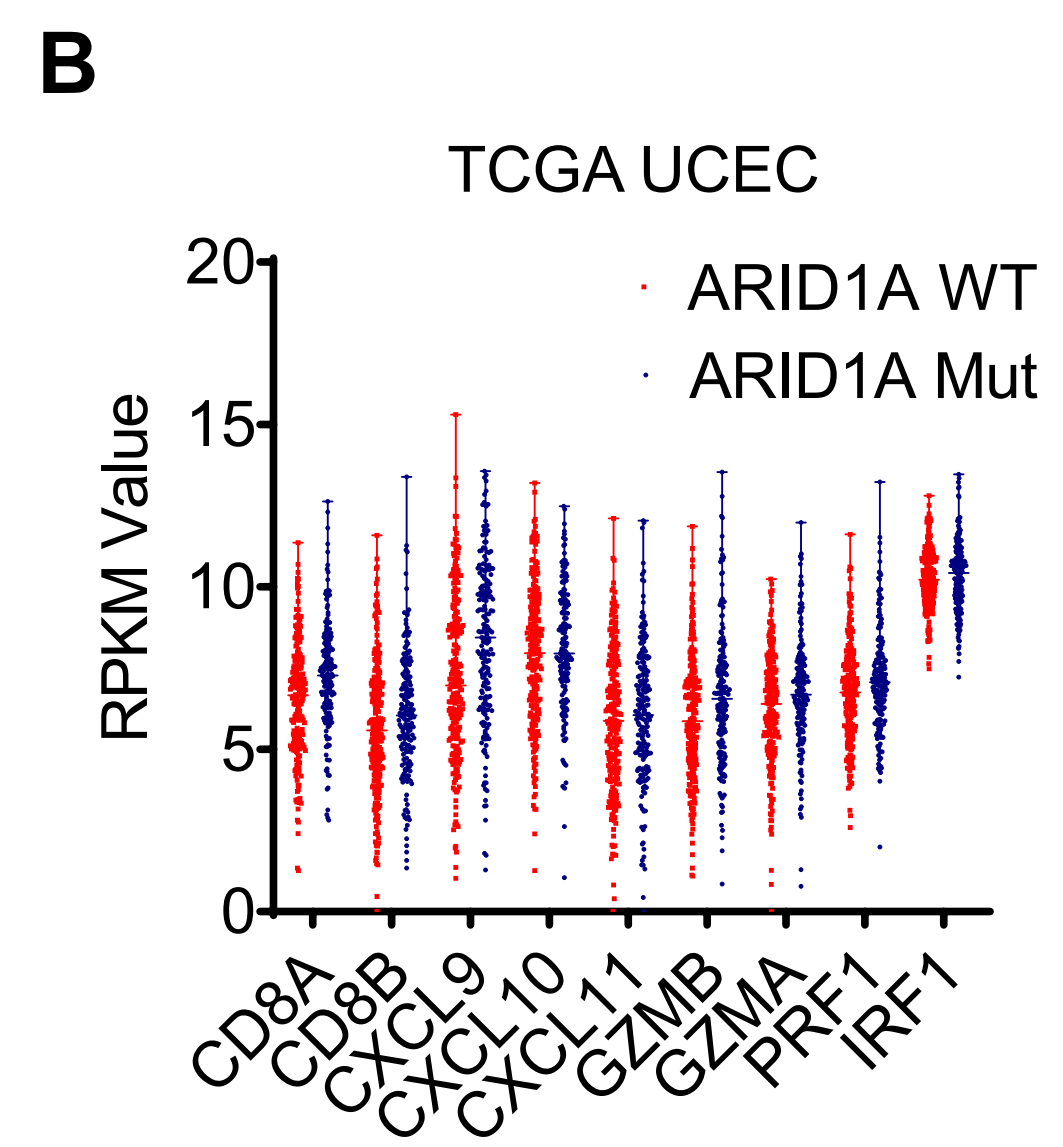
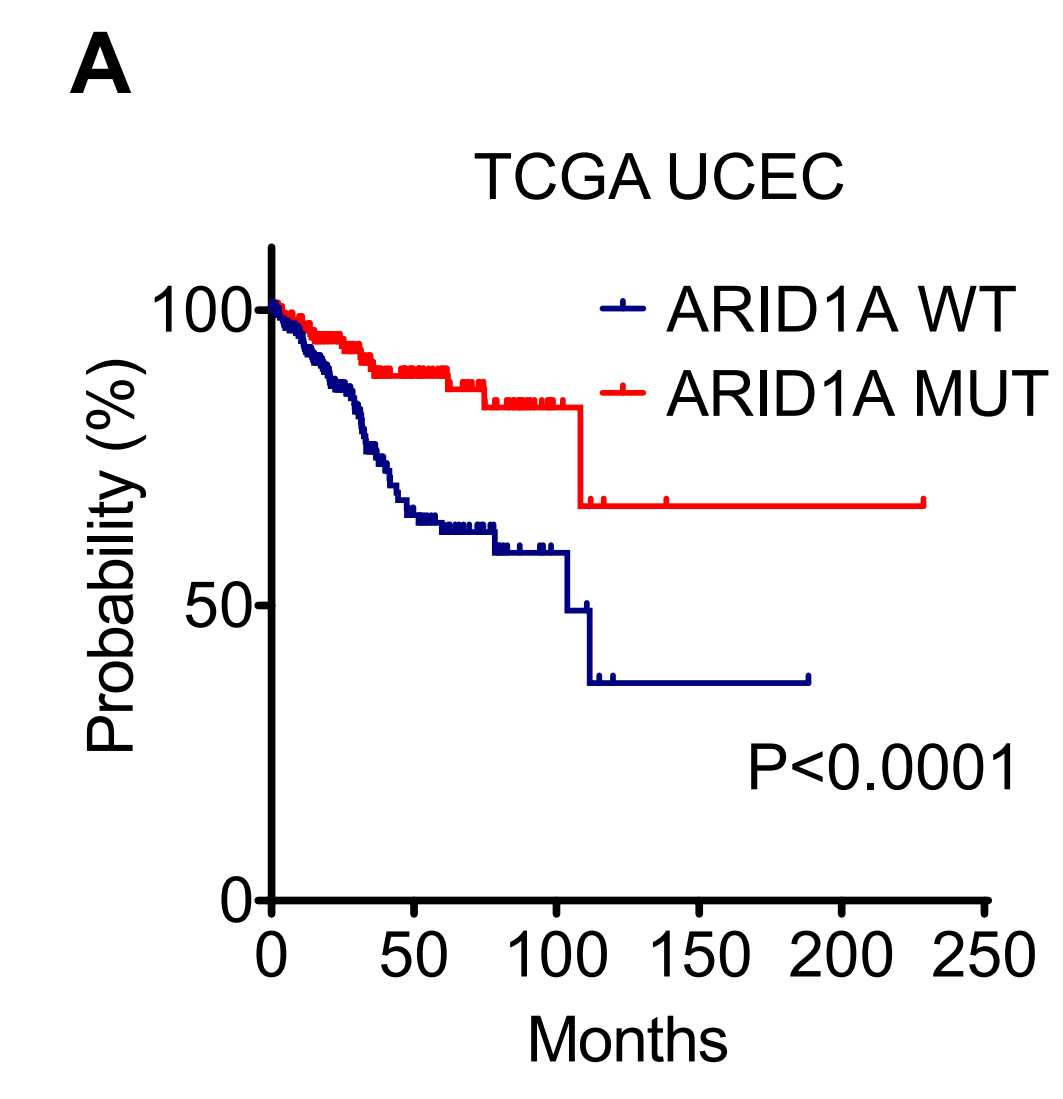
Supplementary Figure 7 ARID1A gene status affects checkpoint therapy

(A-B) Effect of ARID1A on anti-PD-L1 therapy in MC38 bearing mice. Mice bearing shARID1A and control vector expressing MC38 tumors were treated with anti-PD-L1 or isotype. Neoantigen-specific CD8⁺ T cells were analyzed by flow cytometry with adpgk-specific tetramer in tumor infiltrating CD8⁺ T cells (A) and lymph node CD8⁺ T cells (B). One representative of 5 experiments is shown. Mean \pm SD, Mann-Whitney U test, *P < 0.05, **P < 0.01.

(C-E) GSEA pathway analysis in melanoma patients treated with immunotherapy. IFN- γ (C), IFN- α (D), and T cell activation (E) pathways were analyzed and compared in patients with or without immunotherapy-associated clinical benefits.

(F) Effect of anti-PD-1 on biological pathways in melanoma patients. Metastatic melanoma patients (n = 51) were treated with anti-PD-1. 26 and 25 patients manifested clinical benefit (CB) and progressive disease (PD) (NCB), respectively. Differential gene expression between the 2 groups of patients was entered for pathway analysis. DAVID analysis was used to determine these pathways (76). Enriched biological pathways in NCB patients are shown.

Fig. S8



Supplementary Figure 8 ARID1A gene status affects clinical outcome

(A) Overall survival of wild type (n = 243) and mutated (n = 197) ARID1A UCEC patients in TCGA cohort. Log rank test, $P < 0.0001$.

(B) T cell signature genes and IFN- γ signature genes in UCEC patients in TCGA cohort. Specific signature gene expression levels were compared in UCEC patients with wild type (n = 243) and mutated (n = 197) ARID1A.

(C) Overall survival of UCEC patients in TCGA cohort. Patients with POLE and PIK3CA mutations were excluded for analysis. Wild type ARID1A patients (n = 138) and mutated ARID1A patients (n = 65) were compared. Log rank test, $P = 0.24$.

(D) Overall survival of UCEC patients in TCGA cohort. Patients with POLE and PIK3CA mutations and MSI were excluded for analysis. Wild type ARID1A patients (n = 137) and mutated ARID1A patients (n = 53) were compared. Log rank test, $P = 0.67$.

METHODS

Cell Culture, Vectors, and Mutants

Human ovarian clear cell carcinoma cell line OVCA429 (1), human primary high grade serous ovarian carcinoma cell OC8 (2), human primary colon cell line (3, 4), mouse ovarian cancer cell line ID8, and mouse colon cancer cell line MC38 (5, 6) were previously reported. Human colon cell lines DLD-1 and HCT116, and HEK293T cell line were from the American Type Culture Collection (ATCC). Tumor cells were regularly examined for mycoplasma contamination. Cloning of Flag-EZH2, Flag-ARID1A, Myc-EZH2, and their mutated forms was performed as described (7, 8). EZH2 and ARID1A plasmids were generated via the Gateway system. ARID1A mutants were generated by point mutagenesis (Agilent). The plasmids and gene knockout cells were verified by Sanger sequencing at the University of Michigan sequencing core facility.

RNA Extraction, RNA-Sequencing Analysis, GSEA Enrichment Analysis

Total RNA was extracted using Trizol reagent (Invitrogen) and subjected to reverse transcription with AMV reverse transcriptase (Thermo Fisher). Real-time PCR was performed using SYBR green chemistry (Applied Biosystems). Reactions were run on a real-time PCR system (StepOnePlus Real-Time PCR System; Applied Biosystems). The Illumina Ribo-Zero Gold rRNA Removal Kit (Cat# MRZG126) was used for RNA-sequencing library preparation for RNA-sequencing. Sequencing was performed by paired-end 50-mer sequencing in replicates at the University of Michigan sequencing core facility with HiSeq 4000 (Illumina). The sequenced raw reads of each sample were aligned to the human reference genome (GRCh 38 or hg 38 for human, or mm10 for mouse) using HISAT2 (9, 10) with default parameters. The transcriptome was self-merged to allow processing with StringTie (11). Different conditions were compared using ballgown R package (12, 13) with default parameters. The

genome visualization was performed in IGV genome browser (14, 15). The GSEA enrichment analysis was performed under the published protocol (16). Biological pathway analysis was performed with DAVID V6.8 (17).

Stable Gene Knockout and Knockdown Cell Lines

ARID1A knockout cells were generated with CRISPR Technology. ARID1A locus was targeted by control Double Nickase Plasmid or ARID1A Double Nickase Plasmid (h) (Santa Cruz Biotechnology, sc-400469-NIC) using UltraCruz Transfection Reagent and Plasmid Transfection Medium (Santa Cruz Biotechnology), or use CRISPR ARID1A plasmids from Rugang Zhang, (The Wistar Institute, Philadelphia) and Cigall Kadoch (Dana-Farber, Boston). Transfected cells were selected by adding puromycin for 48 hours. Single-cell clones were selected and expanded. Immunoblotting was used to identify knockout cells. We mixed 3 clones from the control group as wild type line, and 3 clones from ARID1A knockout group as ARID1A knockout line. ARID1A knockdown DLD-1 was generated by transfecting si-control (sc-37007) or siARID1A (sc-43628) into DLD-1 cells for 72 hours. ARID1A knockdown primary colon cancer cell line was generated by infecting the cells with sh-control or shARID1A virus (pLenti-CMV-Puro-Luciferase) (1). The cells were then selected with puromycin to get stable knockdown cell line. EZH2 knockdown cells were generated with short-hairpin interfering RNA (shEZH2) as previously reported (5).

Western Blotting

Western blotting was performed as described (2, 5). The following antibodies were used in the experiments, rabbit anti-EZH2 monoclonal antibody (mAb) (#5246, Cell Signaling), anti-EZH2 mAb (BD Biosciences, 612667), anti-ARID1A antibody (PSG3, Santa Cruz, sc-32761), other BAF complex

antibodies (Cell Signaling, #12854), Flag antibody (Sigma, F1804), His antibody (Invitrogen, SK258909), and GST antibody (Millipore, 05-311).

ATAC-seq and NGS Library

Cancer cells were treated with PBS or IFN- γ for 3 hours. Cell nuclei were isolated and subjected to transposase for 30 minutes under active shaking (18, 19). Then, the purified tagged genomic DNA was amplified to generate illumine NGS library with Nextera DNA Sample Preparation Kit (Illumina, #FC-121-1030). The DNA size selection was done with Ampure beads (Beckman Coulter). The library was measured by bioanalyzer. Samples were sequenced with hiSeq 2500 (Illumina). paired-end fastq files were uniquely aligned to hg38 human genome assembly using Novoalign (Novocraft, Inc) with the following parameters: -r None -k -q 13 -k -t 60 -o sam -a CTGTCTCTTATACACATCT, and converted to bam files using SAMtools (1.3.1). Reads mapped to mitochondrial or duplicated reads were removed by SAMtools (1.3.1) and PICARD MarkDuplicates (2.9.0), respectively. Reads were further filtered to identify nucleosome-free, open chromosomal regions. MACS2 was used to call ATAC-seq peaks (20), from which differentially accessible regions were determined by limma (21) and EdgeR (22). The coverage tracks were generated using the program bam2wig (<http://search.cpan.org/dist/Bio-ToolBox/>) with the following parameters:--pe --rpm --span --bw. MEME suite (23) was applied to identify enriched motifs within the IFN- γ -responsive regions.

WES, Mutation Calling and Filtering

Whole exome sequencing was performed in the DNA core of University of Michigan. Sequencing data were aligned to the GRCh38 reference using BWA-MEM (24), with the following non-default settings

“-Y -K 10000000”. For alignment, the GRCh38 1000G reference with alternate contigs and haplotypes was chosen (25). Following alignment, the data were processed using the Sentieon suite of tools (26). The Sentieon processing included indel realignment (equivalent to GATK (27), duplicate removal (equivalent to Picard <http://broadinstitute.github.io/picard/>), and variant calling using TNScope (a haplotype-aware based on GATK3 MuTect (28). The resulting variants which passed significance filtering (FILTER=='PASS') were annotated using vcfAnno (29) with the following information: recurrence in COSMIC (a database of somatic alterations in cancer) (30), recurrence in GNOMAD (a database of germline variants derived from exome and genome sequencing) (31), presence of a variant in dbSNP (a database of germline variation in humans) (32), whether the variant is in a known mutational hotspot (CIVIC) (33), and whether it is annotated as pathogenic in ClinVar (34). Next, the variants were filtered to only include those that: alter the protein sequence (MODERATE or HIGH impact as assessed by VEP (34), are not found in GNOMAD, are not an annotated SNP, are present in either: a manually curated list of genes recurrently mutated in ovarian cancer (Table S4), or a manually curated list of chromatin related genes (Table S3).

Immunoprecipitation

Cells were lysed in NTEP buffer (25mM Tris-HCl pH 7.5, 150mM NaCl, 5mM EDTA, 0.5% NP-40) for 30 minutes at 4°C. 500 ug cell lysate was used to incubate with the EZH2 mAb (Active Motif, #39875) overnight. Then proteinase A Sepharose beads (GE Health) were added for additional 2-hour incubation. After extensive washing, 35 ul SDS loading dye was added into the beads, the beads were boiled for 5 -10 minutes to elute the protein complex. Elutes were then subject to Western blot in 7.5 percent of SDS-PAGE gels.

Chromatin Immunoprecipitation (ChIP)

Cells were harvested 3 hours after IFN- γ (10 ng/mL) treatment. ARID1A (Santa Cruz, sc-32761) ChIP assay was performed per standard protocol (Cell signalling), with SimpleChIP® Plus Enzymatic Chromatin IP Kit (Magnetic Beads). In brief, after cells were fixed and lysed, Micrococcal Nuclease was used to get chromatin fragments. H3K27me3 (abcam, ab6002) and SMARCC1 (Cell signaling, D7F8S) ChIP assays were performed per standard protocol (Millipore), with EZ-ChIP kit (EMD Millipore, 17-371). In brief, after cells were fixed and lysed, sonication was used to shear genomic DNA into fragments. ChIP assays were performed using ChIP-validated antibodies and ChIP-Grade Protein G Beads. After reversal of protein-DNA cross-links and proteinase digestion, DNA was purified using DNA purification columns. ChIP-enriched chromatin was analyzed by real-time PCR with SYBR Green Master Mix, and normalized to the input. The ChIP primers were listed in the supplementary table (Table S8).

***In vivo* Mouse Models**

Six- to eight-week-old NOD.Cg-Prkdcscid Il2rgtm1Wjl/SzJ (NSG) mice and wild type C57BL/6 mice were obtained from the Jackson Laboratory. MC38 colon cancer cells (10^6 or 3×10^6) were subcutaneously injected to the right flank of male mice. Or, luciferase-expressing ID8 ovarian cancer cells (10^6) were injected into the peritoneal cavity of female mice. Anti-PD-L1 and IgG1 isotype control were given intraperitoneally 100 ug/mouse every 3 days from day 3 after tumor cell inoculation. MC38 tumor diameters were measured using calipers. ID8 tumor progression was monitored two times per week using the Xenogen IVIS Spectrum *in Vivo* Bioluminescence Imaging System (PerkinElmer). Tumor load was calculated based on the total flux (photons per second [p/s]). All animal procedures were approved by the IACUC Committee of the University of Michigan.

Flow Cytometry Analysis

Single-cell suspensions were prepared from fresh mouse tumor tissues and tumor draining lymph nodes. Cell suspensions were then overlay on ficoll, lymphocytes were obtained by density gradient centrifuge. For cytokine staining, lymphocytes were incubated with PMA (5ng/ml), Ionomycin (500 ng/ml), Brefeldin A (1: 1000) and Monensin (1: 1000), 4 hours in 37°C CO2 incubator. Anti-CD45 (Clone: 30-F11), anti-CD90 (Clone: 53-2.1), anti-CD4 (Clone: RM4-5) and anti-CD8 (Clone: 53-6.7) were added for 20 minute for surface staining. The cells were then washed and suspend in 1 ml of freshly prepared Permeabilization Buffer A and B, incubate in 4°C overnight. Cells were washed and stained for intracellular cytokine expression. Anti-TNF- α (Clone: MP6-XT22), anti-IL-2 (Clone: JES6-5h4), anti-IFN- γ (Clone: XMG1.2), anti Granzyme B (Clone: GB11).

Gene Correlation Analysis

ARID1A correlation analysis with T cells in TCGA datasets was performed with the TIMER website (<https://cistrome.shinyapps.io/timer/>) (35, 36). The tumor purity was taken into consideration. The datasets with significant impurity were not included in the analysis. Gene expression and mutation status of TCGA PANCAN cohort was downloaded from UCSC xena between February and March of 2019. Recourses of other dataset were indicated in the text or Figure legends.

Statistical Analyses and Patient Survival Analysis

GraphPad Prism6 software (GraphPad Software, Inc.) was used for statistical analysis. Data are presented as mean \pm SD unless indicated in the figure legends. The two-tailed paired student's t-test

was employed to verify whether the difference between two groups is statistically significant. Other statistic methods are indicated in the legends. P-values < 0.05, and 0.01 were considered to be statistically significant.

Kaplan-Meier survival curves of patients with ovarian serous cystadenocarcinoma (37), liver hepatocellular carcinoma, hepatobiliary cancer (38), and pancreatic cancer (38) were illustrated from Cbioportal (<http://www.cbioportal.org/>) (39, 40). Overall survival and disease free survival data of TCGA PANCAN cohort were downloaded from UCSC xena (<http://xena.ucsc.edu>) between February and March of 2019. LogRank test and Gehan-Breslow-Wilcoxon test was used to compute the statistical differences unless indicated in figure legends.

References:

1. Bitler BG, Aird KM, Garipov A, Li H, Amatangelo M, Kossenkov AV, et al. Synthetic lethality by targeting EZH2 methyltransferase activity in ARID1A-mutated cancers. *Nat Med.* 2015;21(3):231-8.
2. Wang W, Kryczek I, Dostal L, Lin H, Tan L, Zhao L, et al. Effector T Cells Abrogate Stroma-Mediated Chemoresistance in Ovarian Cancer. *Cell.* 2016;165(5):1092-105.
3. Kryczek I, Lin Y, Nagarsheth N, Peng D, Zhao L, Zhao E, et al. IL-22(+)/CD4(+) T cells promote colorectal cancer stemness via STAT3 transcription factor activation and induction of the methyltransferase DOT1L. *Immunity.* 2014;40(5):772-84.
4. Nagarsheth N, Peng D, Kryczek I, Wu K, Li W, Zhao E, et al. PRC2 Epigenetically Silences Th1-Type Chemokines to Suppress Effector T-Cell Trafficking in Colon Cancer. *Cancer Res.* 2016;76(2):275-82.
5. Peng D, Kryczek I, Nagarsheth N, Zhao L, Wei S, Wang W, et al. Epigenetic silencing of TH1-type chemokines shapes tumour immunity and immunotherapy. *Nature.* 2015;527(7577):249-53.
6. Lin H, Wei S, Hurt EM, Green MD, Zhao L, Vatan L, et al. Host expression of PD-L1 determines efficacy of PD-L1 pathway blockade-mediated tumor regression. *J Clin Invest.* 2018;128(2):805-15.
7. Jung HY, Jun S, Lee M, Kim HC, Wang X, Ji H, et al. PAF and EZH2 induce Wnt/beta-catenin signaling hyperactivation. *Molecular cell.* 2013;52(2):193-205.

8. Li J, Xi Y, Li W, McCarthy RL, Stratton SA, Zou W, et al. TRIM28 interacts with EZH2 and SWI/SNF to activate genes that promote mammosphere formation. *Oncogene*. 2017.
9. Kim D, Langmead B, and Salzberg SL. HISAT: a fast spliced aligner with low memory requirements. *Nature methods*. 2015;12(4):357-60.
10. Pertea M, Kim D, Pertea GM, Leek JT, and Salzberg SL. Transcript-level expression analysis of RNA-seq experiments with HISAT, StringTie and Ballgown. *Nature protocols*. 2016;11(9):1650-67.
11. Pertea M, Pertea GM, Antonescu CM, Chang TC, Mendell JT, and Salzberg SL. StringTie enables improved reconstruction of a transcriptome from RNA-seq reads. *Nature biotechnology*. 2015;33(3):290-5.
12. Frazee AC, Pertea G, Jaffe AE, Langmead B, Salzberg SL, and Leek JT. Ballgown bridges the gap between transcriptome assembly and expression analysis. *Nature biotechnology*. 2015;33(3):243-6.
13. Fu J FA, Collado-Torres L, Jaffe AE and Leek JT. ballgown: Flexible, isoform-level differential expression analysis. . *R package* 2017;version 2.8.4.
14. Robinson JT, Thorvaldsdottir H, Winckler W, Guttman M, Lander ES, Getz G, et al. Integrative genomics viewer. *Nature biotechnology*. 2011;29(1):24-6.
15. Thorvaldsdottir H, Robinson JT, and Mesirov JP. Integrative Genomics Viewer (IGV): high-performance genomics data visualization and exploration. *Briefings in bioinformatics*. 2013;14(2):178-92.
16. Subramanian A, Tamayo P, Mootha VK, Mukherjee S, Ebert BL, Gillette MA, et al. Gene set enrichment analysis: a knowledge-based approach for interpreting genome-wide expression profiles. *Proceedings of the National Academy of Sciences of the United States of America*. 2005;102(43):15545-50.
17. Dennis G, Jr., Sherman BT, Hosack DA, Yang J, Gao W, Lane HC, et al. DAVID: Database for Annotation, Visualization, and Integrated Discovery. *Genome biology*. 2003;4(5):P3.
18. Buenrostro JD, Giresi PG, Zaba LC, Chang HY, and Greenleaf WJ. Transposition of native chromatin for fast and sensitive epigenomic profiling of open chromatin, DNA-binding proteins and nucleosome position. *Nature methods*. 2013;10(12):1213-8.
19. Corces MR, Trevino AE, Hamilton EG, Greenside PG, Sinnott-Armstrong NA, Vesuna S, et al. An improved ATAC-seq protocol reduces background and enables interrogation of frozen tissues. *Nature methods*. 2017;14(10):959-62.
20. Zhang Y, Liu T, Meyer CA, Eeckhoute J, Johnson DS, Bernstein BE, et al. Model-based analysis of ChIP-Seq (MACS). *Genome biology*. 2008;9(9):R137.
21. Smyth GK. Linear models and empirical bayes methods for assessing differential expression in microarray experiments. *Statistical applications in genetics and molecular biology*. 2004;3:Article3.
22. Robinson MD, McCarthy DJ, and Smyth GK. edgeR: a Bioconductor package for differential expression analysis of digital gene expression data. *Bioinformatics*. 2010;26(1):139-40.
23. Bailey TL, Boden M, Buske FA, Frith M, Grant CE, Clementi L, et al. MEME SUITE: tools for motif discovery and searching. *Nucleic acids research*. 2009;37(Web Server issue):W202-8.
24. Li H. Toward better understanding of artifacts in variant calling from high-coverage samples. *Bioinformatics*. 2014;30(20):2843-51.

25. Regier AA, Farjoun Y, Larson DE, Krasheninina O, Kang HM, Howrigan DP, et al. Functional equivalence of genome sequencing analysis pipelines enables harmonized variant calling across human genetics projects. *Nature communications*. 2018;9(1):4038.
26. Donald Freed RA, Jessica A. Weber, Jeremy S. Edwards. The Sentieon Genomics Tools - A fast and accurate solution to variant calling from next-generation sequence data. *bioRxiv*. 2017.
27. McKenna A, Hanna M, Banks E, Sivachenko A, Cibulskis K, Kernytsky A, et al. The Genome Analysis Toolkit: a MapReduce framework for analyzing next-generation DNA sequencing data. *Genome research*. 2010;20(9):1297-303.
28. Cibulskis K, Lawrence MS, Carter SL, Sivachenko A, Jaffe D, Sougnez C, et al. Sensitive detection of somatic point mutations in impure and heterogeneous cancer samples. *Nature biotechnology*. 2013;31(3):213-9.
29. Pedersen BS, Layer RM, and Quinlan AR. Vcfanno: fast, flexible annotation of genetic variants. *Genome biology*. 2016;17(1):118.
30. Forbes SA, Bhamra G, Bamford S, Dawson E, Kok C, Clements J, et al. The Catalogue of Somatic Mutations in Cancer (COSMIC). *Current protocols in human genetics*. 2008;Chapter 10:Unit 10 1.
31. Lek M, Karczewski KJ, Minikel EV, Samocha KE, Banks E, Fennell T, et al. Analysis of protein-coding genetic variation in 60,706 humans. *Nature*. 2016;536(7616):285-91.
32. Sherry ST, Ward MH, Kholodov M, Baker J, Phan L, Smigielski EM, et al. dbSNP: the NCBI database of genetic variation. *Nucleic acids research*. 2001;29(1):308-11.
33. Griffith M, Spies NC, Krysiak K, McMichael JF, Coffman AC, Danos AM, et al. CIViC is a community knowledgebase for expert crowdsourcing the clinical interpretation of variants in cancer. *Nature genetics*. 2017;49(2):170-4.
34. Landrum MJ, Lee JM, Benson M, Brown GR, Chao C, Chitipiralla S, et al. ClinVar: improving access to variant interpretations and supporting evidence. *Nucleic acids research*. 2018;46(D1):D1062-D7.
35. Li B, Severson E, Pignon JC, Zhao H, Li T, Novak J, et al. Comprehensive analyses of tumor immunity: implications for cancer immunotherapy. *Genome biology*. 2016;17(1):174.
36. Riaz N, Havel JJ, Makarov V, Desrichard A, Urba WJ, Sims JS, et al. Tumor and Microenvironment Evolution during Immunotherapy with Nivolumab. *Cell*. 2017;171(4):934-49 e15.
37. Cancer Genome Atlas Research N. Integrated genomic analyses of ovarian carcinoma. *Nature*. 2011;474(7353):609-15.
38. Zehir A, Benayed R, Shah RH, Syed A, Middha S, Kim HR, et al. Mutational landscape of metastatic cancer revealed from prospective clinical sequencing of 10,000 patients. *Nat Med*. 2017;23(6):703-13.
39. Cerami E, Gao J, Dogrusoz U, Gross BE, Sumer SO, Aksoy BA, et al. The cBio cancer genomics portal: an open platform for exploring multidimensional cancer genomics data. *Cancer Discov*. 2012;2(5):401-4.
40. Gao J, Aksoy BA, Dogrusoz U, Dresdner G, Gross B, Sumer SO, et al. Integrative analysis of complex cancer genomics and clinical profiles using the cBioPortal. *Science signaling*. 2013;6(269):p11.

Supplemental Table 8**Primers for RT-PCR**

Target Gene	Forward Primer	Reverse Primer
Human GAPDH	GTCTCCTCTGACTTCAACAGCG	ACCACCCTGTTGCTGTAGCCAA
Human CXCL9	GTGGTGTTCTTTTCCTCTTGGG	ACAGCGACCCTTTTCTCACTAC
Human CXCL10	CTCCAGTCTCAGCACCATGA	GCTCCCCTCTGGTTTTAAGG
Mouse ACTB	CATTGCTGACAGGATGCAGAAGG	TGCTGGAAGGTGGACAGTGAGG
Mouse CXCL10	AATGAGGGCCATAGGGAAGC	AGCCATCCACTGGGTAAAGG
Mouse CXCL9	GAGCAGTGTGGAGTTCGAGG	TCCGGATCTAGGCAGGTTTG

Primers for ChIP

Target Gene	Forward Primer	Reverse Primer
CXCL9 TSS	TGCACTCCAATCAGAACCAG	CCAATACAGGAGTGACTTGGAAC
CXCL10 TSS	TCCCTCCCTAATTCTGATTGG	AGCAGAGGGAAATTCCGTAAC

Fig. 2A

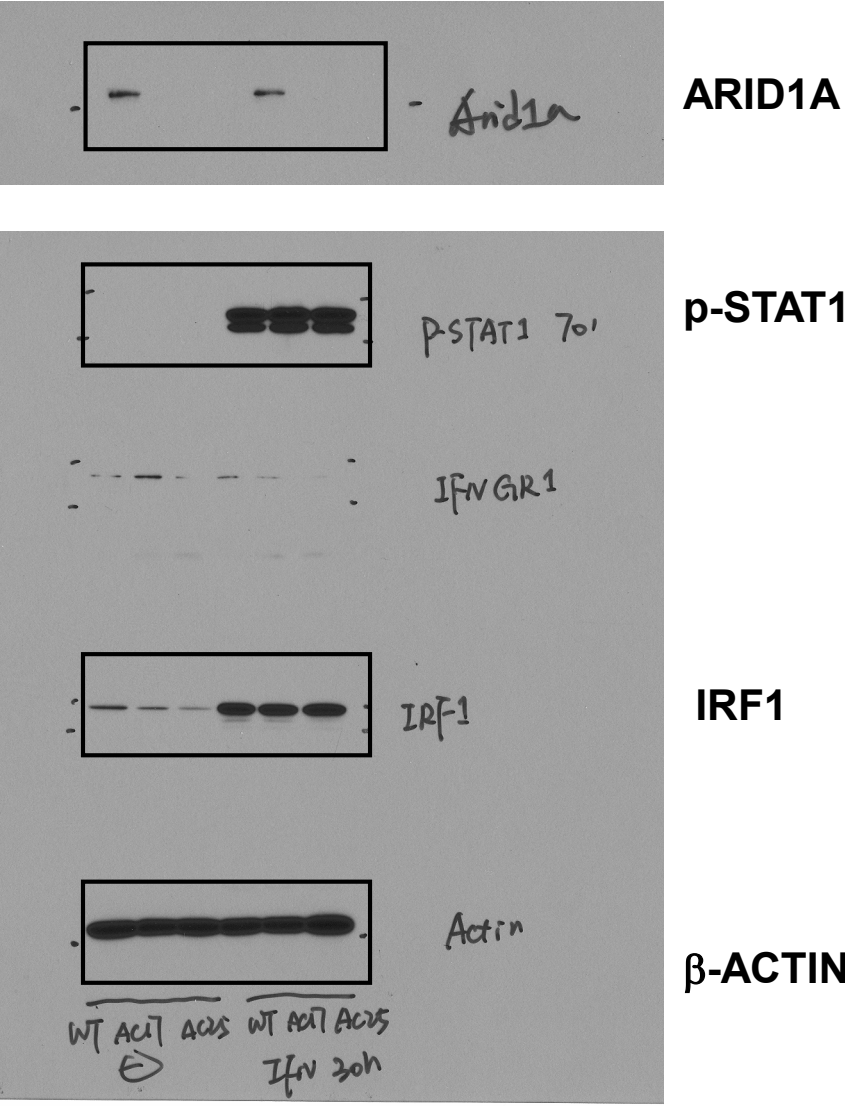


Fig. S2A

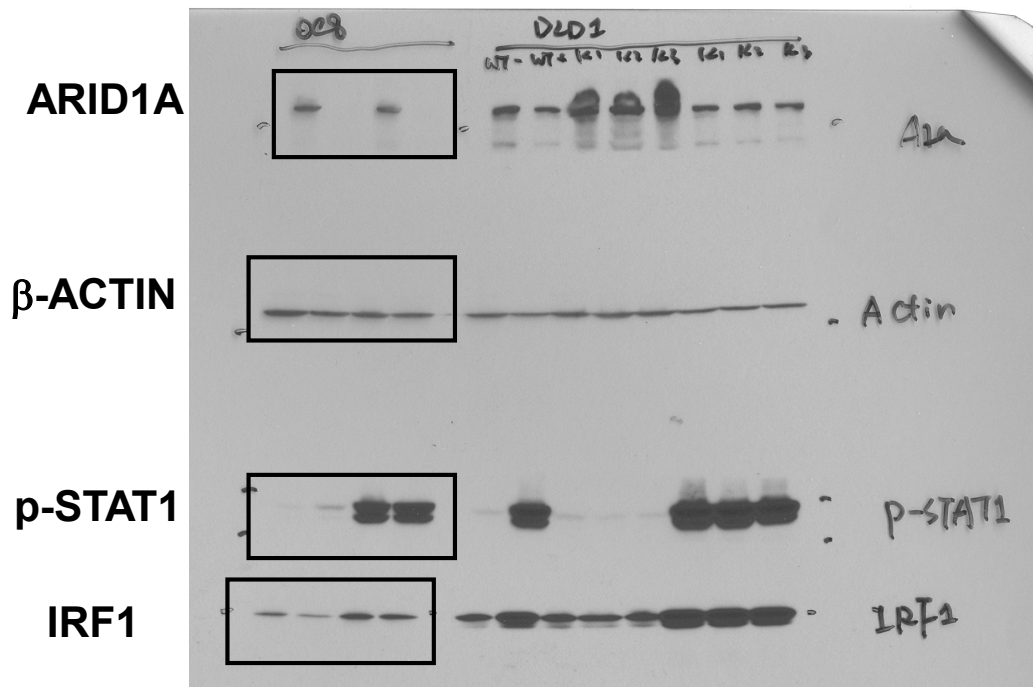


Fig. S2B

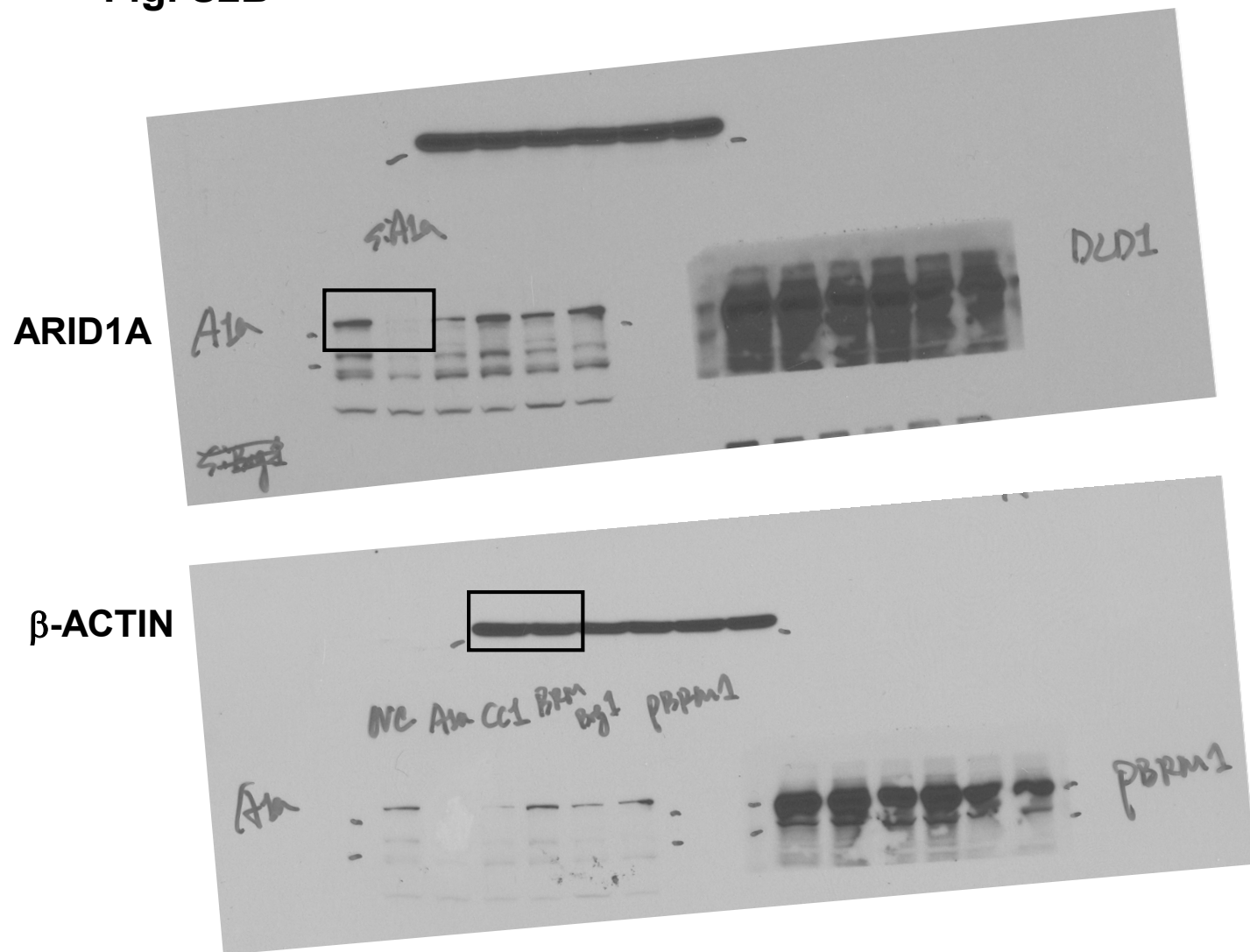


Fig. 4A

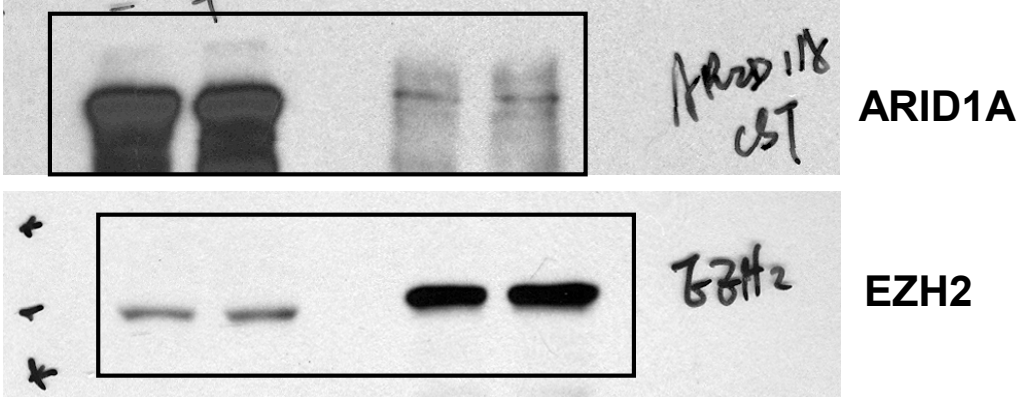


Fig. 4C

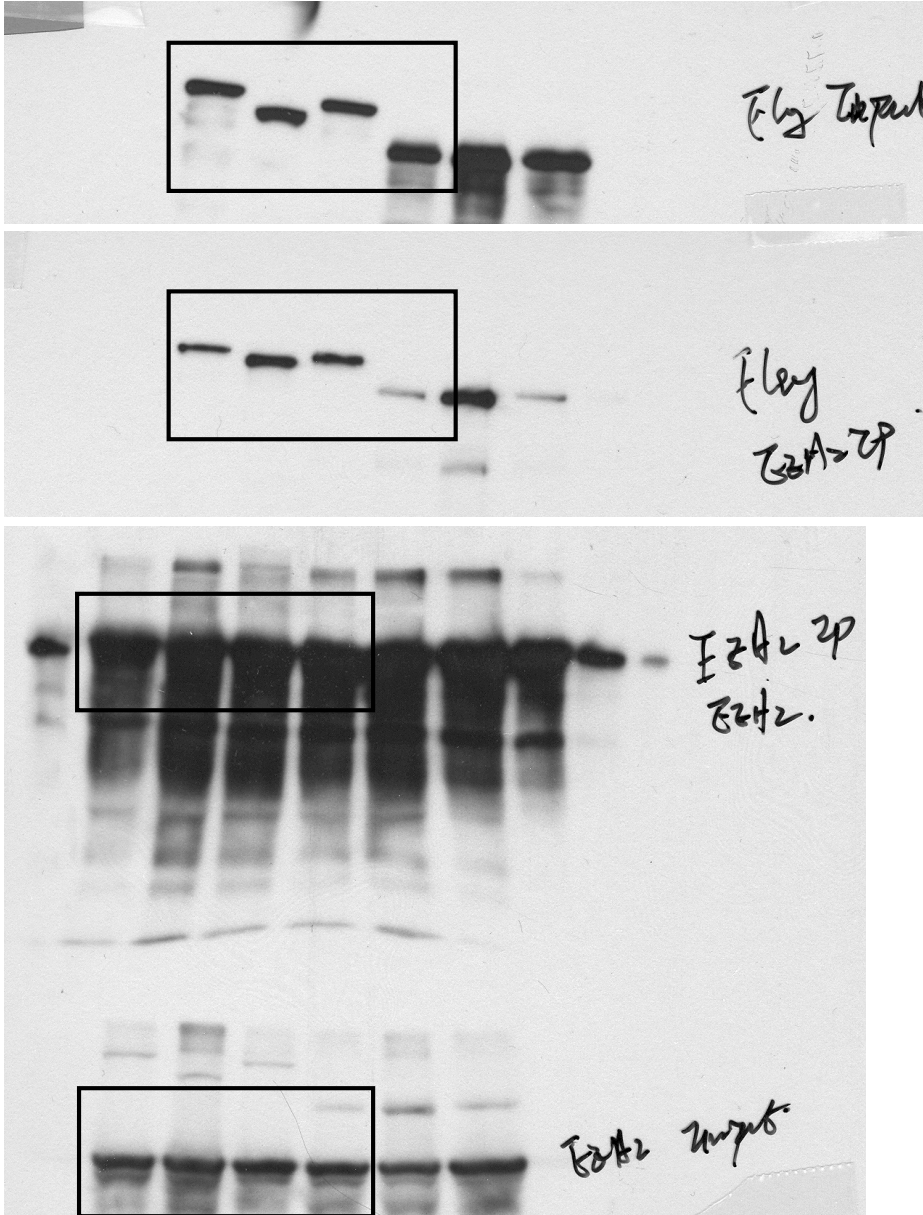


Fig. 4D

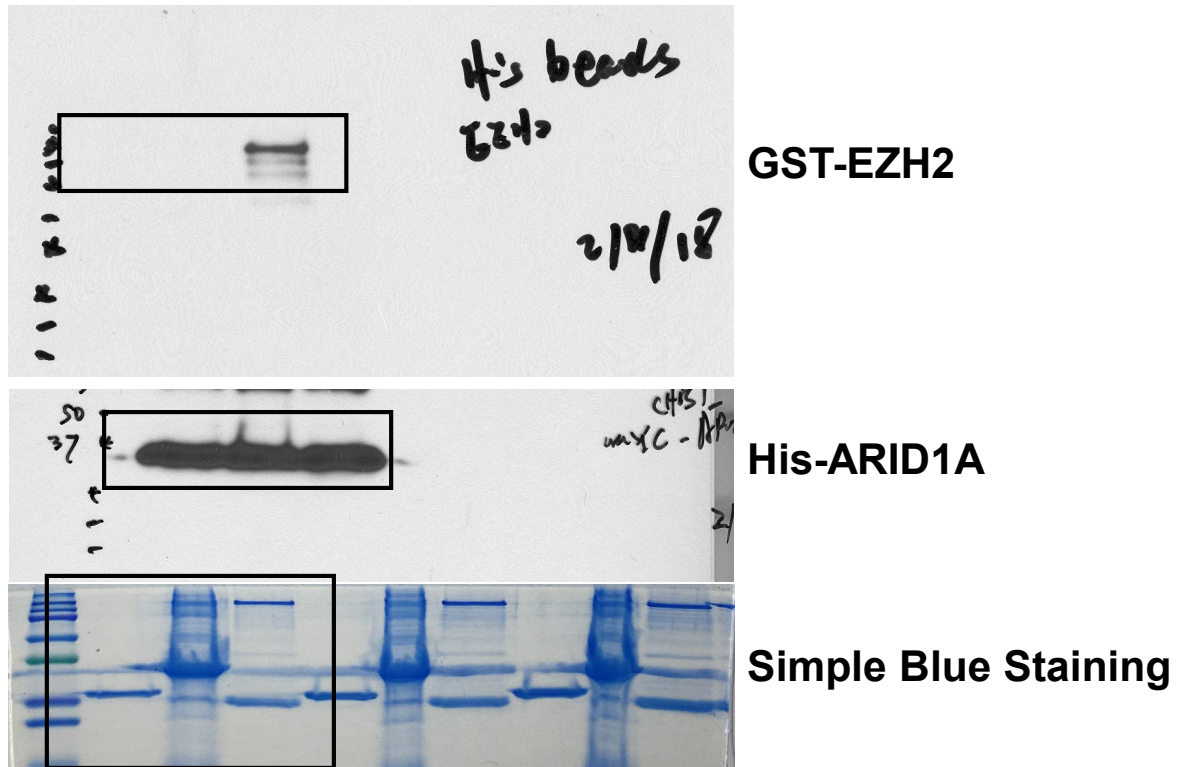


Fig. 4F

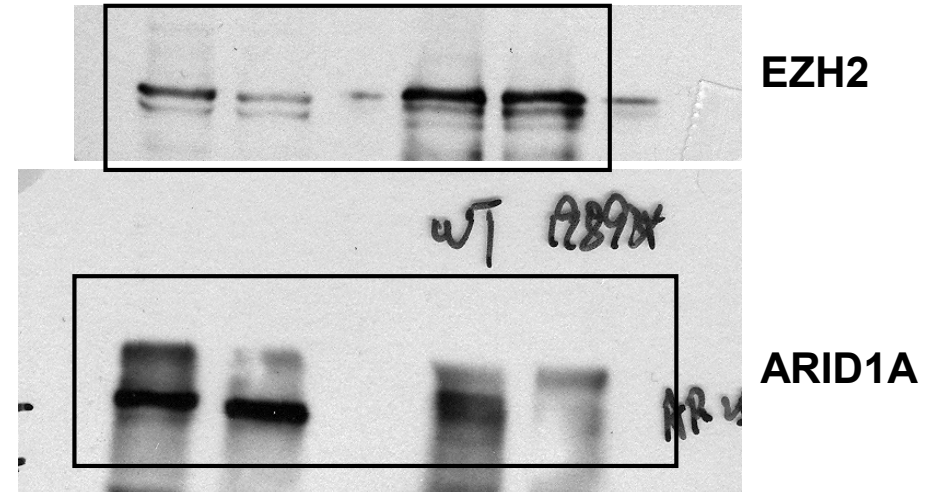


Fig. S4A

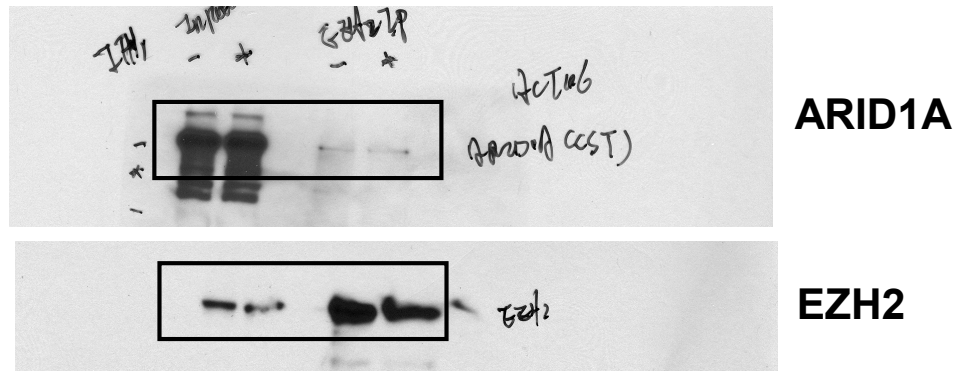


Fig. S4B

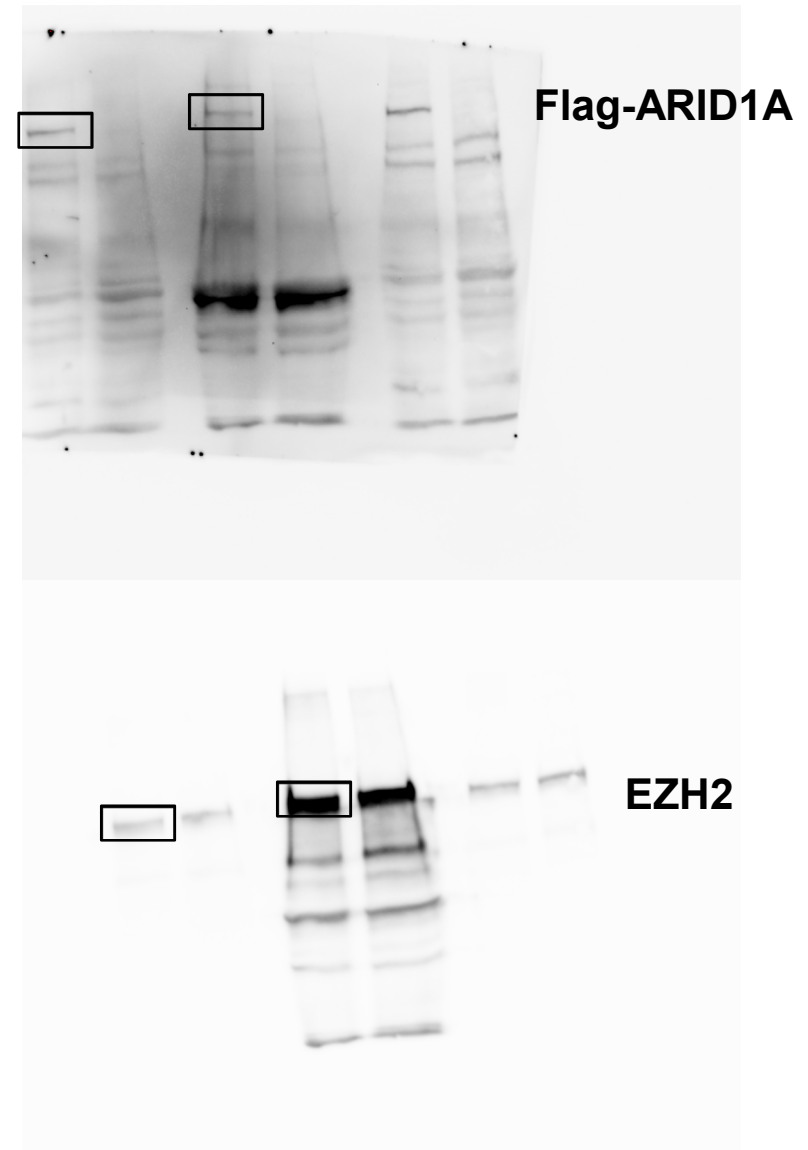
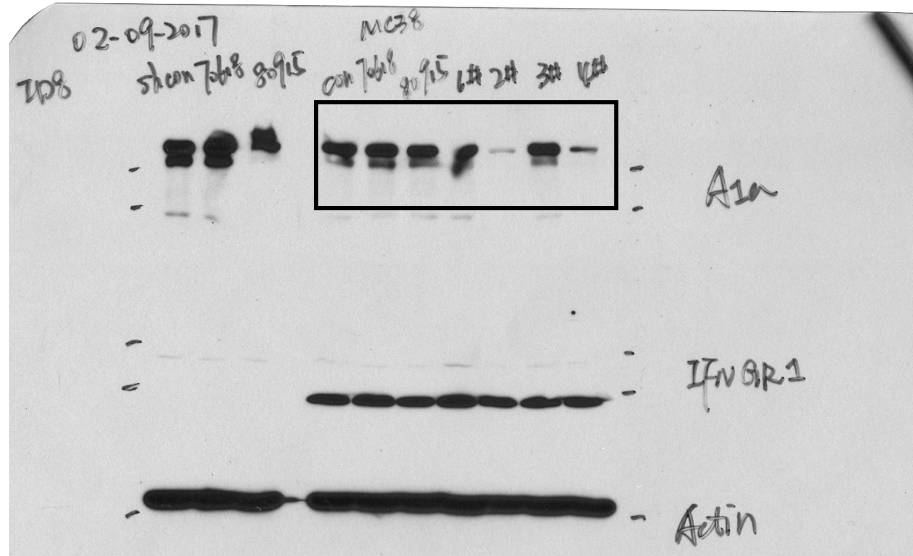


Fig. S5C

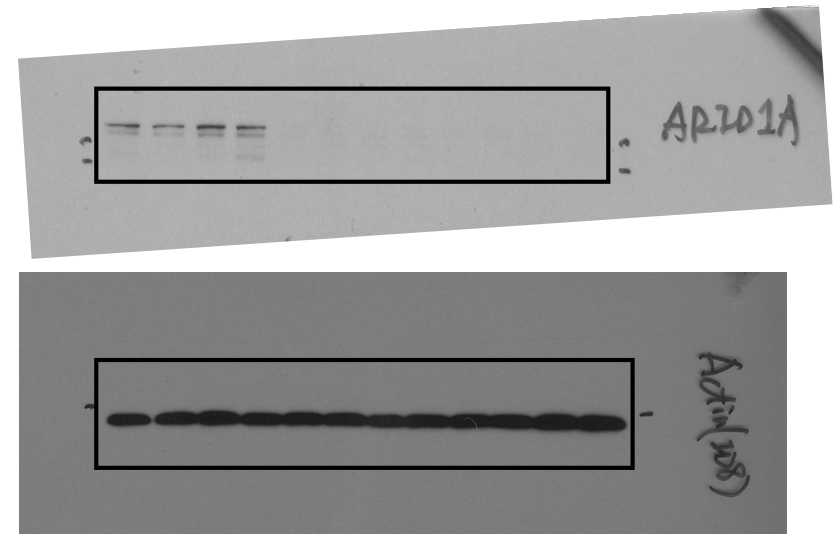
ARID1A



ARID1A

Fig. S5H

β -ACTIN



β -ACTIN

